AD-A149 842 A SOLUTION METHOD FOR LARGE DEFORMATION CONTACT PROBLEMS(U) MASSACHUSETTS INST OF TECH CAMBRIDGE DEPT OF MECHANICAL ENGINEERING K J BATHE OCT 84 BRL-CR-534 1/1

UNCLASSIFIED DAAK11-82-K-0015 F/G 20/11 NL

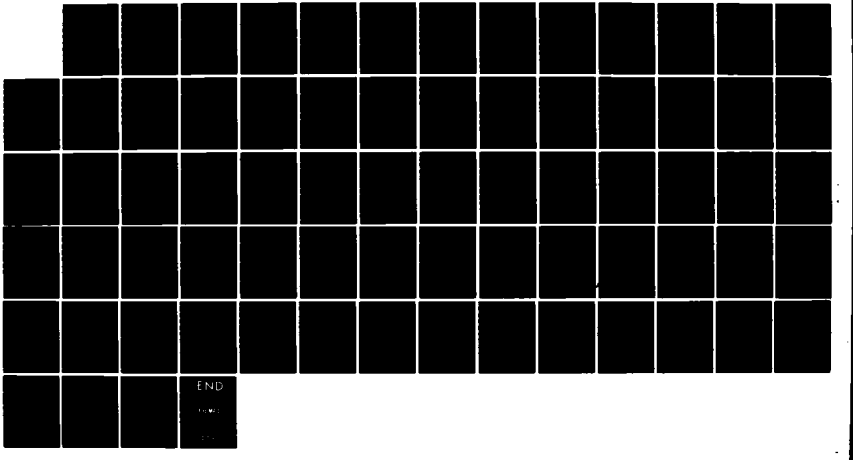

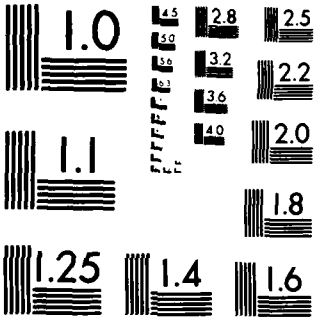

12

BRL

AD-A149 842

AD

CONTRACT REPORT BRL-CR-534

A SOLUTION METHOD FOR LARGE DEFORMATION CONTACT PROBLEMS

Prepared by

Massachusetts Institute of Technology
Mechanical Engineering Department
Cambridge, Massachusetts 02139

October 1984

US ARMY BALLISTIC RESEARCH LABORATORY
ABERDEEN PROVING GROUND, MARYLAND

Destroy this report when it is no longer needed.
Do not return it to the originator.

Additional copies of this report may be obtained from the National Technical Information Service, U. S. Department of Commerce, Springfield, Virginia 22161.

The findings in this report are not to be construed as an official Department of the Army position, unless so designated by other authorized documents.

The use of trade names or manufacturers' names in this report does not constitute indorsement of any commercial product.

UNCLASSIFIED

SECURITY CLASSIFICATION OF THIS PAGE *(When Data Entered)*

REPORT DOCUMENTATION PAGE		READ INSTRUCTIONS BEFORE COMPLETING FORM
1. REPORT NUMBER CONTRACT REPORT BRL-CR-534	2. GOVT ACCESSION NO. AD-A149842	3. RECIPIENT'S CATALOG NUMBER
4. TITLE *(and Subtitle)* A SOLUTION METHOD FOR LARGE DEFORMATION CONTACT PROBLEMS		5. TYPE OF REPORT & PERIOD COVERED Contract Report Aug. 1982 to Aug. 1983 6. PERFORMING ORG. REPORT NUMBER
7. AUTHOR(s) Klaus-Jurgen Bathe		8. CONTRACT OR GRANT NUMBER(s) DAAK11-82-K-0015
9. PERFORMING ORGANIZATION NAME AND ADDRESS Massachusetts Institute of Technology Mech. Eng. Dept.; Rm. 3-356 Cambridge, MA 02139		10. PROGRAM ELEMENT, PROJECT, TASK AREA & WORK UNIT NUMBERS 1L161102AH43
11. CONTROLLING OFFICE NAME AND ADDRESS US Army Ballistic Research Laboratory ATTN: AMXBR-OD-ST Aberdeen Proving Ground, MD 21005-5066		12. REPORT DATE October 1984 13. NUMBER OF PAGES 68
14. MONITORING AGENCY NAME & ADDRESS*(if different from Controlling Office)*		15. SECURITY CLASS. *(of this report)* Unclassified 15a. DECLASSIFICATION/DOWNGRADING SCHEDULE

16. DISTRIBUTION STATEMENT *(of this Report)*

Approved for public release; distribution unlimited.

17. DISTRIBUTION STATEMENT *(of the abstract entered in Block 20, if different from Report)*

18. SUPPLEMENTARY NOTES

This work was performed under contract to the Blast Dynamics Branch, Terminal Ballistic Division, U.S. Army Ballistic Research Laboratory, AMXBR-TBD, Dr. Joseph M. Santiago, Contracting Officer's Representative.

19. KEY WORDS *(Continue on reverse side if necessary and identify by block number)*

Contact Problem Algorithm
Finite Element Structural Analysis
Coulomb Friction Sliding and Sticking
Lagrange Multiplier Contact Forces
Implicit Solution Technique
Full Newton-Raphson Equilibrium Iteration
ADINA Finite Element Program

20. ABSTRACT *(Continue on reverse side if necessary and identify by block number)*

A solution procedure for the analysis of planar and axisymmetric contact problems involving sticking, frictional sliding and separation under large deformations is presented. The contact conditions are imposed using the total potential of the contact forces with the geometric compatibility conditions, which leads to contact system matrices and force vectors. Some key aspects of the procedure are the gradient matrix corresponding to sliding, the use of distributed tractions on the contact segments for deciding

DD FORM 1 JAN 73 1473 EDITION OF 1 NOV 65 IS OBSOLETE

UNCLASSIFIED

SECURITY CLASSIFICATION OF THIS PAGE *(When Data Entered)*

20. whether a node is sticking, sliding or releasing and the evaluation of the nodal point contact forces. The solutions to various sample problems are presented to demonstrate the applicability of the algorithm.

TABLE OF CONTENTS

LIST OF ILLUSTRATIONS

LIST OF ILLUSTRATIONS (cont'd.)

1. INTRODUCTION

Much progress has been made during the recent years in the development of computational capabilities for general analysis of certain nonlinear effects in solids and structures. In each of these developments, quite naturally, the first step was the demonstration of some ideas and possibilities for the analyses under consideration, and then the research and development for reliable and general techniques was undertaken. This second step proved in many cases much more difficult, and in the case of capabilities for analysis of contact problems has yielded few general results.

Although some of the first complex contact problems have been solved using the finite element method quite some time ago [1-3], and much interest exists in the research and solution of contact problems [see, for ex. refs. 4-15], there is still a great deal of effort necessary for the development of a reliable, general, and cost-effective algorithm for the practical analysis of such problems. This is largely due to the fact that the analysis of contact problems is computationally extemely difficult, despite the relatively simple mechanics theory used for these problems. Much of the difficulty lies in that the boundary conditions of the bodies under consideration are not known prior to the analysis but they depend on the solution variables.

The aim in our research is the development of a solution algorithm for analysis of general contact conditions which shall include the possibilities to analyse,

- contact between flexible-flexible and rigid-flexible bodies,
- sticking or sliding conditions (with or without friction),
- large relative motions between bodies,
- repeated contact and separation between the bodies.

Since the large deformation motion of the individual bodies can in many cases be analysed already quite effectively [16], an algorithm of the above nature will certainly enlarge, very significantly, the currently available computational capabilities for practical nonlinear analyses. The objective in this paper is to present our first research results towards the above aim.

In this paper we consider the large deformation of two-dimensional planar or axisymmetric bodies in contact and in static conditions. The algorithm we present contains the following major ingredients:

- The total potential of the contact forces is included in the variational formulation to enforce the geometric compatibilities along the contact surfaces.

- In the region of contact, surface tractions are evaluated from the externally applied forces and nodal point forces equivalent (in the virtual work sense) to the current element stresses.

- The surface tractions between nodal points (on the element segments) are employed to decide whether a nodal point is in sticking or sliding contact, or is releasing.

- The number of equations due to the contact conditions is dynamically adjusted to solve two equations for each node in contact if the node is in sticking condition, and one equation if the node is in sliding condition.

Because of the highly nonlinear contact conditions to be analysed, the success of the algorithm largely depends on an effective formulation with special attention to details. We believe that the gradient matrix used when sliding conditions are analysed and the segment approach employed to decide on the contact conditions are two important and key aspects of our algorithm.

In the next two sections we present the formulation of the algorithm and the important numerical details. We have implemented the solution method in the computer program ADINA [17], and in Section 4 we give the solutions to various sample problems. These serve to demonstrate the applicability of and also the assumptions used in the algorithm.

2. FORMULATION OF CONTACT PROBLEM

Figure 1 shows schematically the problem we consider. This figure shows two generic bodies which we arbitrarily denote as contactor and target. In the finite element solution, the contactor contains the finite element boundary nodes that come into contact with the target segments or nodes. Although only two bodies are shown to come into contact, the algorithm can analyse the contact conditions between a number of bodies.

The basic conditions of contact along the contact surfaces are that no material overlap can occur, and as a result, contact forces are developed that act along the region of contact upon the target and the contactor. These forces are equal and opposite. The normal tractions can only exert compressive action, and the tangential tractions satisfy a law of frictional resistance.

The Friction Law Used. Much research effort is currently focussed upon the development of appropriate friction laws and the mechanics using these laws to predict motion along slip surfaces, e.g., [11, 18, 19].

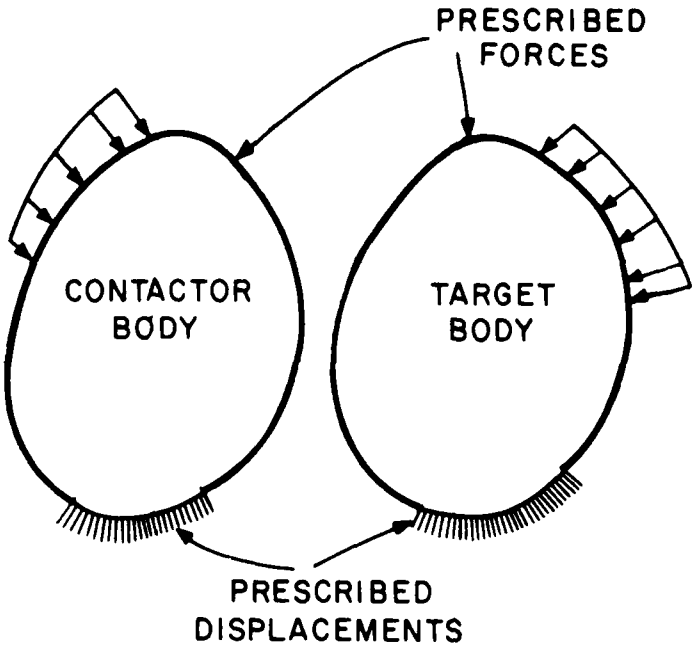

a) Condition prior to contact

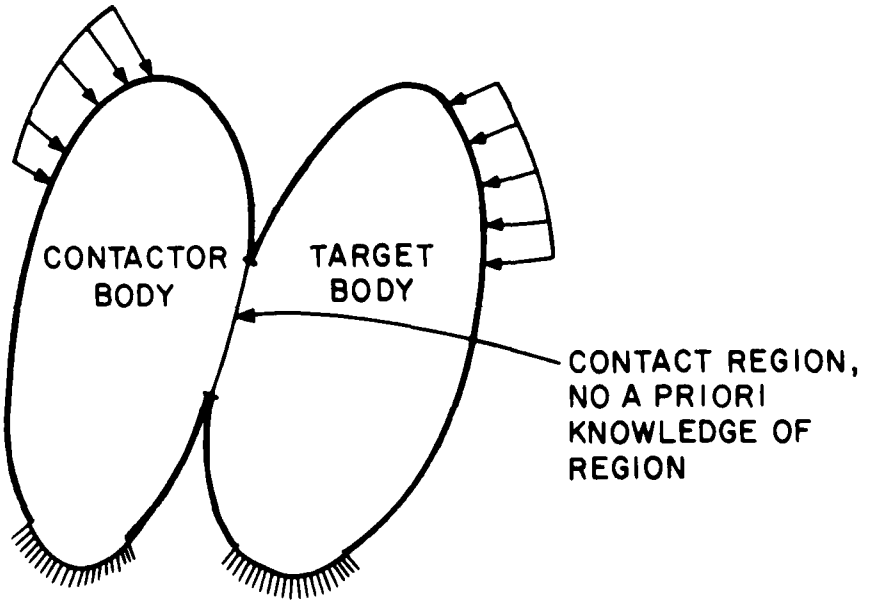

b) Condition at contact

Figure 1. Schematic representation of problem considered

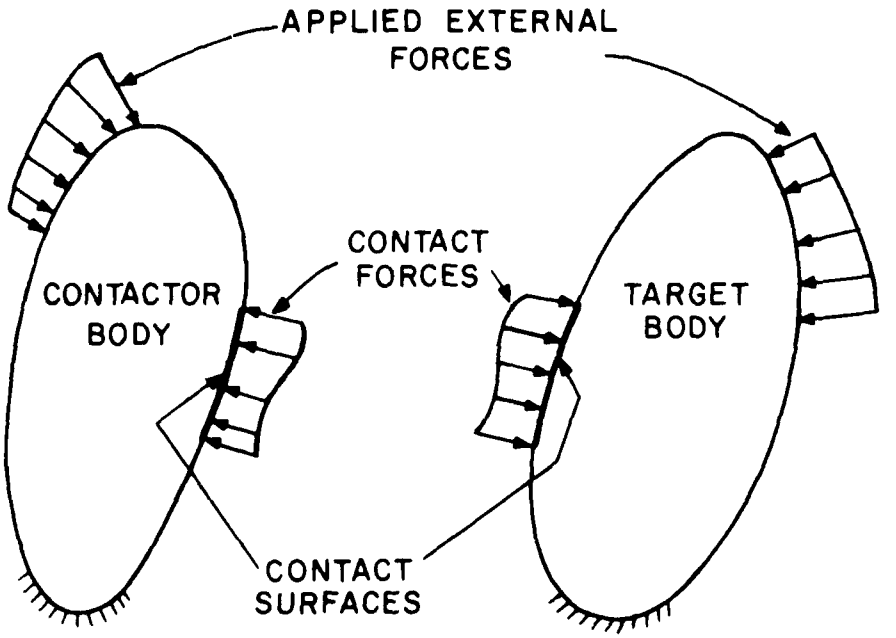

c) Forces acting on contactor and target bodies

Figure 1 Schematic representation of problem considered

Considering the development of our contact algorithm, we therefore should use a friction model that is physically realistic and that we can extend in further developments, and as more refined models become available. These criteria are fulfilled using Coulomb's law of friction with μ_s the static coefficient of friction and μ_d the dynamic (or kinetic) coefficient of friction [20, pp. 53-64].

Consider the particles initially in contact: those belonging to the target body and those of the contactor. If t_t represents the developed tangential tractions along the contact surfaces, we assume that there is no relative motion between two adjacent particles on the contactor and the target in contact, as long as $|t_t| \leq \mu_s t_n$, where t_n is the compressive normal traction (assumed positive). The maximum traction of static friction is the smallest force necessary to start motion. During motion the magnitude of the tangential traction resisted by friction is $\mu_d t_n$, with $\mu_d \leq \mu_s$. The motion continues as long as the frictional traction is developed to equal the dynamic friction $\mu_d t_n$ that can actually be resisted. Once the developed tangential traction drops below the dynamic friction, the relative motion between the contactor and target particles ceases until such time that again the developed tangential traction exceeds the frictional capacity.

We may note that with this friction law, we neglect any elasticity between the particles in contact and assume a rigid-plastic contact behavior. Refinements of this friction law would entail the use of rate and state variables, as discussed, for example in [19].

Considering our finite element formulation of the above frictional conditions, we should note the following two important points. Firstly, although rigid-plastic behavior is assumed between particles in contact, the two-dimensional finite element discretization around the contact region can represent nonlinear, e.g., elastic-plastic, material conditions. Secondly, the above friction law is in our finite element formulation satisfied in a global sense over each individual contact segment (as discussed in Section 3) consistent with the level of finite element discretization used.

Some Preliminaries. For the formulation of our contact solution algorithm we use the incremental procedures – including the notation – presented in ref. [16, Chapter 6] and recognize that for each of the bodies, the contact conditions can be imposed by adding to the usual variational indicator, the total potential of the contact forces with the constraint of compatible boundary displacements. Hence, in the formulation we invoke stationarity of the following functional,

$$\pi_1 = \pi - \sum_k W_k \qquad (1)$$

where π is the usual (incremental) total potential leading to the incremental equilibrium equations without contact conditions, and $\sum_k W_k$ is the incremental potential of the contact forces. This term can be interpreted as a Lagrange multiplier contribution to impose the contact conditions. In the following sections we concentrate on the evaluation of W_k for a generic node k on the contactor surface (and of the corresponding nodes on the target surface) in sticking and sliding conditions.

Assume that in the incremental solution, the response at time t has been calculated and that (i-1) iterations have been performed to calculate the solution at time $t+\Delta t$. The formulation of the governing equations is achieved by establishing W_k for the next iteration (i). We repeat that this contribution is the only change in the incremental equilibrium equations presented in ref. [16, Chapter 6].

Figure 2 shows a generic region of contact considered which satisfies the contact conditions. We note that the displacements and coordinates are interpolated linearly between adjacent nodes on the contact surfaces of the bodies,(+) and that some of the nodes can be in contact whereas others are still (or again) in separation. Also, based on the assumptions along the region of contact, the contactor nodes cannot be within the region of the target body, but the target nodes can be inside or outside the contactor body. This point requires particular attention when modeling a problem for use of the contact algorithm.

2.1 Potential of Contact Forces for Sticking Contact

A contactor node k is assumed to be in sticking contact under two conditions:

a) The contactor node has penetrated the target body in iteration (i-1) whereas it was not in contact after iteration (i-2).

(+) Actually, as will become apparent, the contact solution algorithm can also be employed when the contactor and/or target bodies are discretized using parabolic elements (see Sections 4.1 and 4.4).

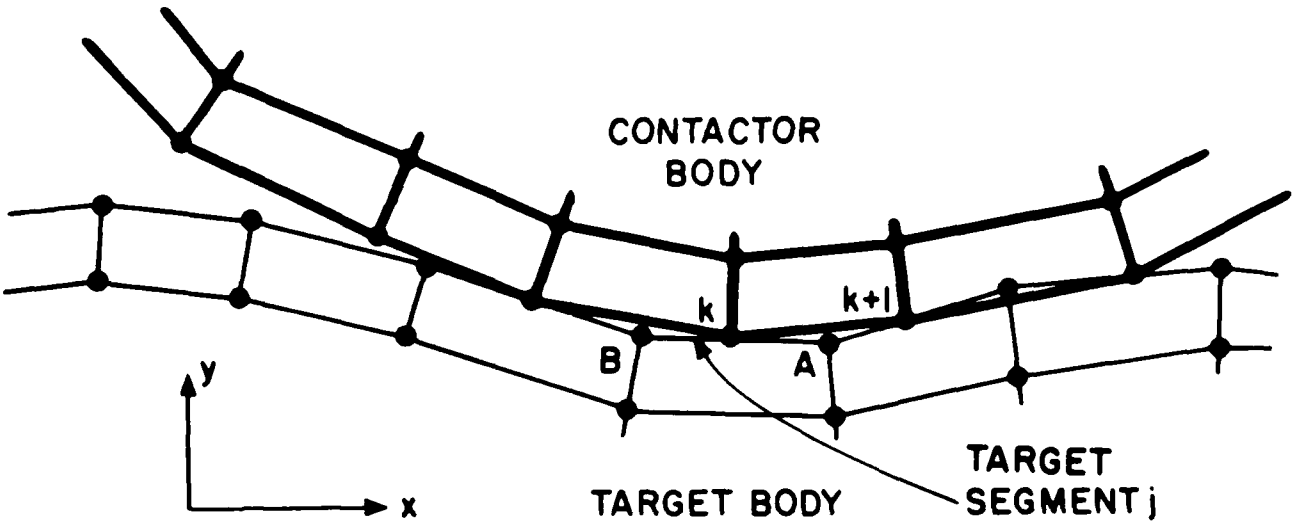

Figure 2 Finite element discretization in contact region. Nodal point numbers on contactor surface increase in direction such that when moving from k to k+1 the contactor body is on the left hand side.

b) The frictional resistance during contact is sufficient to prevent sliding.

In case (a) the contact force at node k at the beginning of iteration (i) is zero and the contact force is generated during iteration (i) when the overlap is eliminated.

Figure 3 shows how node k has come into contact with the target segment j formed by nodes A and B, where

$^{t+\Delta t}\underline{x}_k^{(i-1)}$, $^{t+\Delta t}\underline{x}_A^{(i-1)}$, $^{t+\Delta t}\underline{x}_B^{(i-1)}$ = current global coordinates of nodes k, A, B, respectively, after iteration (i-1) for the equilibrium configuration corresponding to time $t+\Delta t$ (†)

$^{t+\Delta t}\underline{x}_C^{(i-1)}$ = current global coordinates of the assumed physical point of contact of node k

$\underline{\Delta}_k^{(i-1)}$ = overlap

$d_j^{(i-1)}$ = length of segment j

r, s = local isoparametric coordinate system along target surface

$\underline{n}_r$, $\underline{n}_s$ = unit vectors along local axes r, s on target segment, respectively, with respect to the global reference frame; updated during each iteration (but for ease of notation the superscript (i-1) is not given)

(†) Note that, as in Chapter 6 of ref. [16], the left superscript "t+Δt" on a variable denotes the configuration t+Δt in the incremental solution, and does not imply a dynamic analysis [16, p. 309].

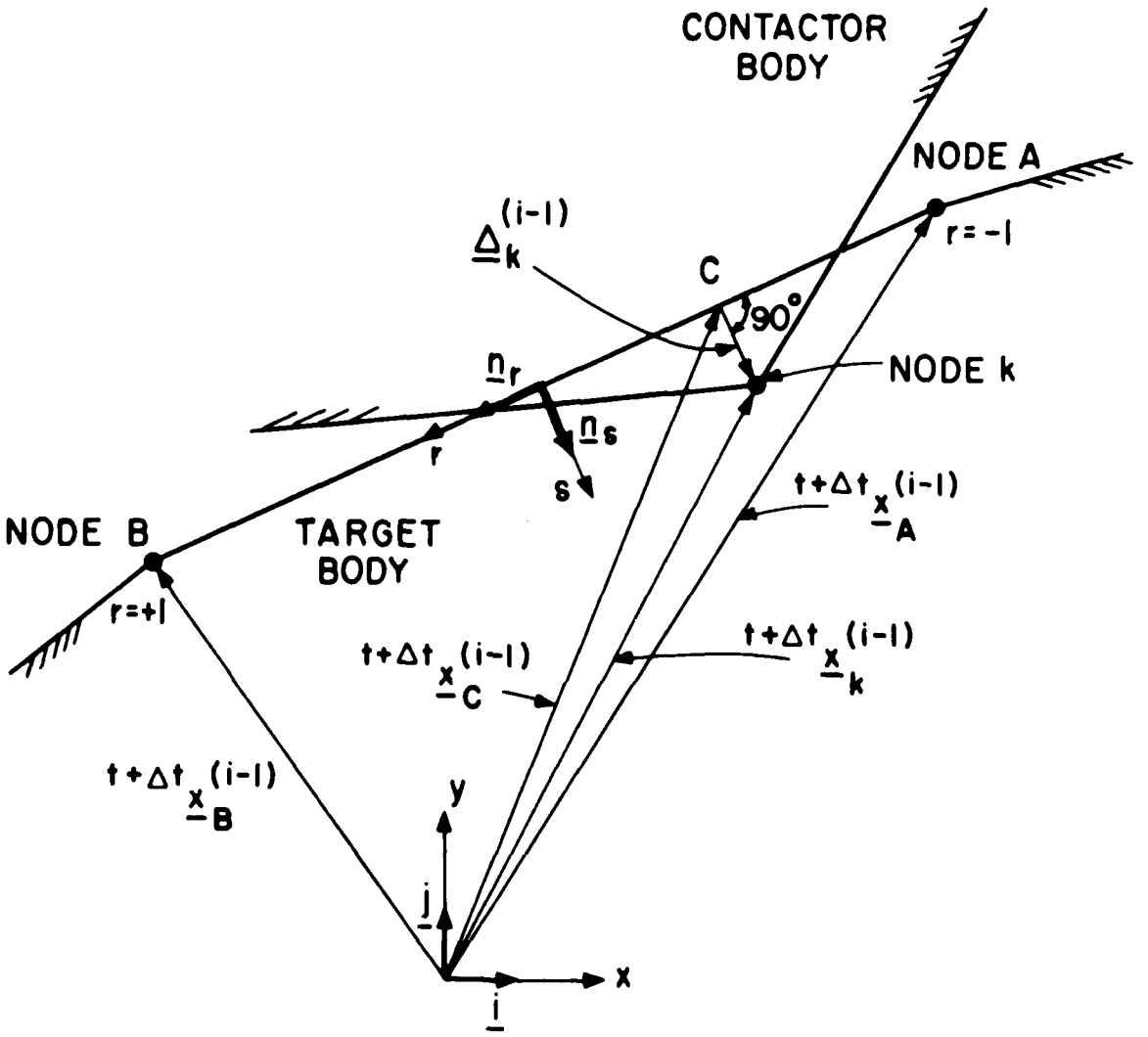

a) Geometric variables

Figure 3. Definition of variables for segment j

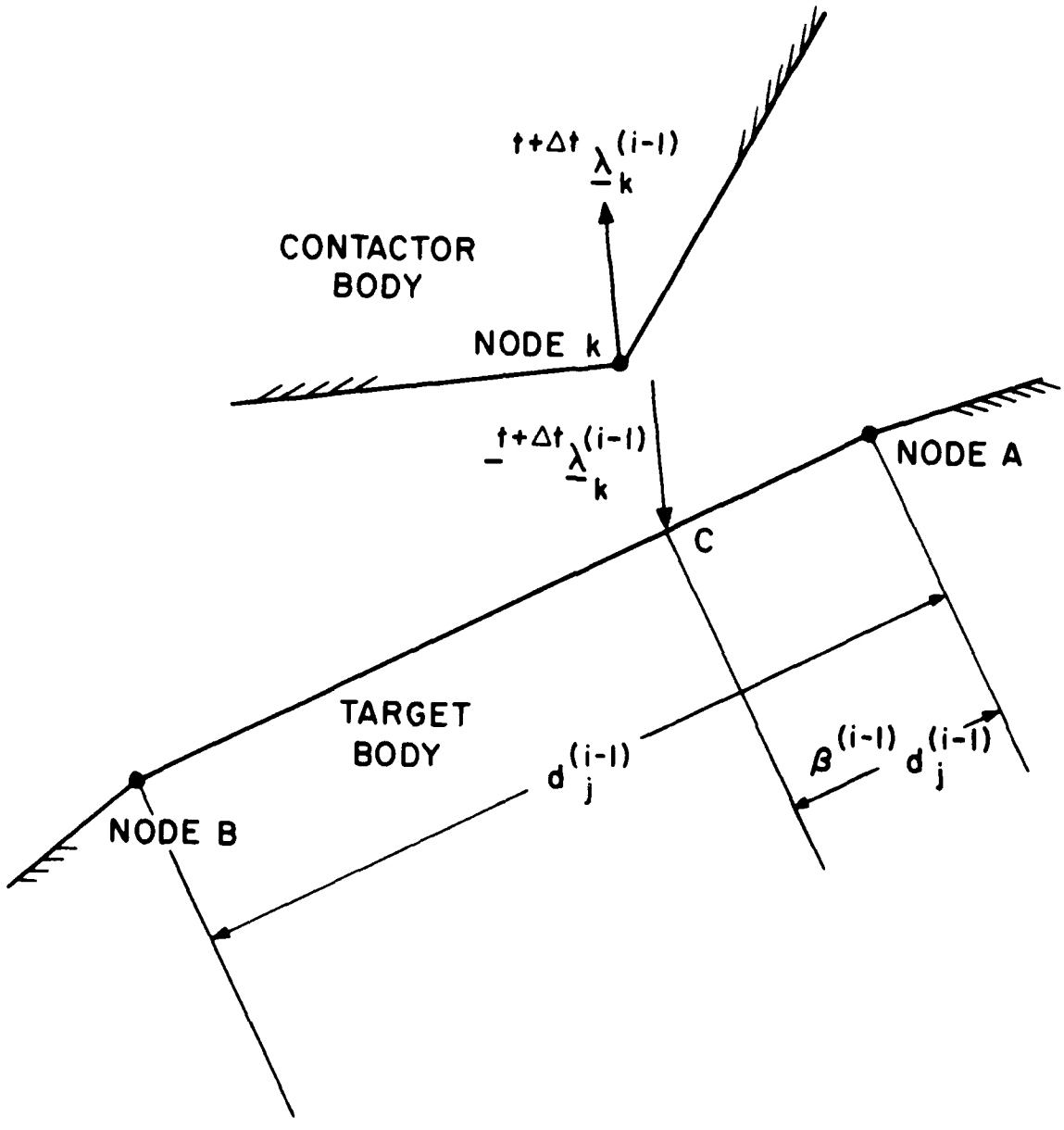

b) Contact Forces

Figure 3 Definition of variables for segment j

$\underline{i}, \underline{j}$ = unit vectors along global x, y coordinate axes

$\beta^{(i-1)}$ = parameter of location of physical point of contact

At node k we have a contact force that we denote here as ${}^{t+\Delta t}\underline{\lambda}_k^{(i-1)}$, but whose evaluation we discuss in detail in Section 3, where

$$ {}^{t+\Delta t}\underline{\lambda}_k^{(i-1)} = {}^{t+\Delta t}\lambda_{kx}^{(i-1)}\,\underline{i} + {}^{t+\Delta t}\lambda_{ky}^{(i-1)}\,\underline{j} \quad . \tag{2} $$

Note that the components of ${}^{t+\Delta t}\underline{\lambda}_k^{(i-1)}$ appear in the vector ${}^{t+\Delta t}\underline{R}_c^{(i-1)}$ of Eq. (18).

Also, from geometry,

$$ \underline{\Delta}_k^{(i-1)} = {}^{t+\Delta t}\underline{x}_k^{(i-1)} - {}^{t+\Delta t}\underline{x}_C^{(i-1)} \tag{3} $$

$$ d_j^{(i-1)} = \underline{n}_r^T \left[{}^{t+\Delta t}\underline{x}_B^{(i-1)} - {}^{t+\Delta t}\underline{x}_A^{(i-1)} \right] \tag{4} $$

$$ \begin{aligned} \beta^{(i-1)} &= \underline{\bar{n}}_r^T \left[{}^{t+\Delta t}\underline{x}_C^{(i-1)} - {}^{t+\Delta t}\underline{x}_A^{(i-1)} \right] \\ &= \underline{\bar{n}}_r^T \left[\left({}^{t+\Delta t}\underline{x}_k^{(i-1)} - \underline{\Delta}_k^{(i-1)} \right) - {}^{t+\Delta t}\underline{x}_A^{(i-1)} \right] \end{aligned} \tag{5} $$

where,

$$ \underline{\bar{n}}_r = \frac{\underline{n}_r}{d_j^{(i-1)}} = \bar{n}_{rx}\underline{i} + \bar{n}_{ry}\underline{j} \quad . \tag{6} $$

And we have for target segment j, the forces equivalent to $-{}^{t+\Delta t}\underline{\lambda}_k^{(i-1)}$,

$$ {}^{t+\Delta t}\underline{\lambda}_A^{(i-1)} = -(1-\beta^{(i-1)})\ {}^{t+\Delta t}\underline{\lambda}_k^{(i-1)} \quad . \tag{7} $$

$$ {}^{t+\Delta t}\underline{\lambda}_B^{(i-1)} = -\beta^{(i-1)}\ \ {}^{t+\Delta t}\underline{\lambda}_k^{(i-1)} \quad . \tag{8} $$

Let the displacement increments at nodes k, A, B in iteration (i) be $\Delta\underline{u}_k^{(i)}$, $\Delta\underline{u}_A^{(i)}$, $\Delta\underline{u}_B^{(i)}$ respectively. These displacements are such that the overlap $\underline{\Delta}_k^{(i-1)}$ is eliminated. Also, if contact was already present, the point of contact C for node k is the same during each iteration, hence $\beta^{(i)} = \beta^{(i-1)}$. The potential W_k due to the contact force at node k and the corresponding reactions is in iteration i,

$$ W_k = {}^{t+\Delta t}\underline{\lambda}_k^{(i)T}\ (\Delta\underline{u}_k^{(i)} + \underline{\Delta}_k^{(i-1)}) + {}^{t+\Delta t}\underline{\lambda}_A^{(i)T}\ \Delta\underline{u}_A^{(i)} + {}^{t+\Delta t}\underline{\lambda}_B^{(i)T}\ \Delta\underline{u}_B^{(i)} \quad . \tag{9} $$

Also

$$ {}^{t+\Delta t}\underline{\lambda}_k^{(i)} = {}^{t+\Delta t}\underline{\lambda}_k^{(i-1)} + \Delta\underline{\lambda}_k^{(i)} \tag{10} $$

where $\Delta\underline{\lambda}_k^{(i)}$ is the change in the contact force at node k. Using Eqs. (7) to (10) we obtain

$$W_k = {}^{t+\Delta t}\underline{\lambda}_k^{(i-1)T}[(\Delta\underline{u}_k^{(i)} + \underline{\Delta}_k^{(i-1)}) - (1-\beta^{(i-1)})\ \Delta\underline{u}_A^{(i)} - \beta^{(i-1)}\ \Delta\underline{u}_B^{(i)}]$$

$$+ \Delta\underline{\lambda}_k^{(i)T}[(\Delta\underline{u}_k^{(i)} + \underline{\Delta}_k^{(i-1)}) - (1-\beta^{(i-1)})\ \Delta\underline{u}_A^{(i)} - \beta^{(i-1)}\ \Delta\underline{u}_B^{(i)}] \quad . \tag{11}$$

This potential is considered for all contactor nodes k that are in sticking contact.

2.2 Potential of Contact Forces for Sliding Contact

A contactor node k is assumed to be in sliding contact if according to the criteria given in Section 3, the tangential force exceeds the frictional capacity. The calculation of total potential for the sliding contact condition is more involved than for sticking contact because the parameter of location, $\beta^{(i-1)}$, changes during iteration (i) to a new value $\beta^{(i)}$. However, the frictional force is assumed to remain constant during the iteration. Using Eqs. (7) to (9) with $\beta^{(i)}$ we have,

$$W_k = {}^{t+\Delta t}\underline{\lambda}_k^{(i)T}[(\Delta\underline{u}_k^{(i)} + \underline{\Delta}_k^{(i-1)}) - (1-\beta^{(i)})\ \Delta\underline{u}_A^{(i)} - \beta^{(i)}\ \Delta\underline{u}_B^{(i)}] \tag{12}$$

where

$$\beta^{(i)} = \beta^{(i-1)} + \Delta\beta^{(i)} \tag{13}$$

and from Eq. (5) we obtain, by linearization,

$$\Delta\beta^{(i)} = \pm\ \underline{\tilde{n}}_r^T[(\Delta\underline{u}_k^{(i)} + \underline{\Delta}_k^{(i-1)}) - (1-\beta^{(i-1)})\Delta\underline{u}_A^{(i)} - \beta^{(i-1)}\ \Delta\underline{u}_B^{(i)}] \quad . \tag{14}$$

Also, for sliding

$$t+\Delta t\underline{\lambda}_k^{(i)} = t+\Delta t\underline{\lambda}_k^{(i-1)} + \Delta\underline{\lambda}_k^{(i)} \tag{15}$$

$$\Delta\underline{\lambda}_k^{(i)} = -\Delta\lambda_s^{(i)}\ \underline{n}_s \tag{16}$$

where $\Delta\lambda_s^{(i)}$ is the change in the magnitude of the normal component of $t+\Delta t\underline{\lambda}_k^{(i-1)}$. The negative sign in Eq. (16) is used because an increase in the normal force is acting into the opposite direction of $\underline{n}_s$.

Substituting from Eqs. (13) to (16) into Eq. (12) we obtain

$$\begin{aligned} W_k \doteq\ & t+\Delta t\underline{\lambda}_k^{(i-1)^T}\left[(\Delta\underline{u}_k^{(i)} + \underline{\Delta}_k^{(i-1)}) - (1-\beta^{(i-1)})\,\Delta\underline{u}_A^{(i)} - \beta^{(i-1)}\,\Delta\underline{u}_B^{(i)}\right] \\ & + t+\Delta t\underline{\lambda}_k^{(i-1)^T}\,(\Delta\beta^{(i)})\,(\Delta\underline{u}_A^{(i)} - \Delta\underline{u}_B^{(i)}) \\ & + \Delta\lambda_s^{(i)}\left\{-\underline{n}_s^T[(\Delta\underline{u}_k^{(i)} + \underline{\Delta}_k^{(i-1)}) - (1-\beta^{(i-1)})\,\Delta\underline{u}_A^{(i)} - \beta^{(i-1)}\,\Delta\underline{u}_B^{(i)}]\right\} \end{aligned} \tag{17}$$

where we neglected $(\Delta\lambda_s^{(i)})(\Delta\beta^{(i)})$ terms.

This potential is considered for all nodes k that are in sliding contact.

2.3 Governing Finite Element Equations

The incremental finite element equations of motion including contact conditions are generated by substituting from Eqs. (11) and (17) into Eq. (1) and invoking stationarity, $\delta\pi_1 = 0$. Hence, we obtain, using the usual procedures.

$$\left\{ \begin{bmatrix} {}^{t+\Delta t}\underline{K}^{(i-1)} & \underline{0} \\ \underline{0} & \underline{0} \end{bmatrix} + \begin{bmatrix} {}^{t+\Delta t}\underline{K}_c^{(i-1)} \end{bmatrix} \right\} \begin{bmatrix} \Delta\underline{U}^{(i)} \\ \Delta\underline{\lambda}^{(i)} \end{bmatrix}$$

$$= \begin{bmatrix} {}^{t+\Delta t}\underline{R} \\ \underline{0} \end{bmatrix} - \begin{bmatrix} {}^{t+\Delta t}\underline{F}^{(i-1)} \\ \underline{0} \end{bmatrix} + \begin{bmatrix} {}^{t+\Delta t}\underline{R}_c^{(i-1)} \\ {}^{t+\Delta t}\underline{\Delta}_c^{(i-1)} \end{bmatrix} \tag{18}$$

where,

$\Delta\underline{U}^{(i)}$ = Vector of incremental displacements in iteration (i); of dimension (NEQx1).

$\Delta\underline{\lambda}^{(i)}$ = Vector of increments in contact forces in iteration (i); (NEQCx1).

${}^{t+\Delta t}\underline{K}^{(i-1)}$ = Usual tangent stiffness matrix including material and geometric nonlinearities after iteration (i-1); (NEQxNEQ).

${}^{t+\Delta t}\underline{K}_c^{(i-1)}$ Contact stiffness matrix, for the effect of contact conditions after iteration (i-1); (NEQTxNEQT).

${}^{t+\Delta t}\underline{F}^{(i-1)}$ = Vector of nodal point forces equivalent to element stresses after iteration (i-1); (NEQx1).

${}^{t+\Delta t}\underline{R}$ = Vector of total applied external forces at time t+Δt; (NEQx1).

${}^{t+\Delta t}\underline{R}_c^{(i-1)}$ = Vector of updated contact forces after iteration (i-1), (NEQx1).

${}^{t+\Delta t}\underline{\Delta}_c^{(i-1)}$ = Vector of overlaps (NEQCx1).

NEQ = Total number of displacement degrees of freedom.

NEQC = Total number of incremental contact constraint equations

= 2x (total number of nodes in sticking contact) + (total number of nodes in sliding contact).

NEQT = NEQ + NEQC

Each contactor node k contributes to ${}^{t+\Delta t}\underline{K}_c^{(i-1)}$, ${}^{t+\Delta t}\underline{R}_c^{(i-1)}$ and ${}^{t+\Delta t}\underline{\Delta}_c^{(i-1)}$. Consider these terms for a single contactor node since the contributions for a number of nodes are obtained by addition of the individual contributions using the direct stiffness method [16].

In the case of sticking contact, the first term in Eq. (11) results in the vector ${}^{t+\Delta t}\underline{R}_c^{(i-1)}$, whereas the second term gives the contact stiffness matrix ${}^{t+\Delta t}\underline{K}_c^{(i-1)}$ and overlap vector ${}^{t+\Delta t}\underline{\Delta}_c^{(i-1)}$,

$$
{}^{t+\Delta t}\underline{R}_c^{(i-1)} = \begin{bmatrix} {}^{t+\Delta t}\lambda_{kx}^{(i-1)} \\ {}^{t+\Delta t}\lambda_{ky}^{(i-1)} \\ -(1-\beta^{(i-1)})\ {}^{t+\Delta t}\lambda_{kx}^{(i-1)} \\ -(1-\beta^{(i-1)})\ {}^{t+\Delta t}\lambda_{ky}^{(i-1)} \\ -\beta^{(i-1)}\ {}^{t+\Delta t}\lambda_{kx}^{(i-1)} \\ -\beta^{(i-1)}\ {}^{t+\Delta t}\lambda_{ky}^{(i-1)} \end{bmatrix} \qquad (19)
$$

$$
{}^{t+\Delta t}\underline{\Delta}_c^{(i-1)} = \begin{bmatrix} \Delta_{kx}^{(i-1)} \\ \Delta_{ky}^{(i-1)} \end{bmatrix} \qquad (20)
$$

and

$$
{}^{t+\Delta t}\underline{K}_c^{(i-1)} = \left[\begin{array}{cc|c} & & \begin{matrix} -1 & 0 \\ 0 & -1 \\ 1-\beta^{(i-1)} & 0 \\ 0 & 1-\beta^{(i-1)} \\ \beta^{(i-1)} & 0 \\ 0 & \beta^{(i-1)} \end{matrix} \\ \multicolumn{2}{c|}{\underline{0}} & \\ & & \begin{matrix} 0 & 0 \\ & 0 \end{matrix} \\ \multicolumn{2}{c|}{\text{symmetric}} & \end{array}\right] \qquad (21)
$$

where the corresponding solution vector is in detail,

$$
\begin{bmatrix} \Delta\underline{U}^{(i)} \\ \Delta\underline{\lambda}^{(i)} \end{bmatrix} = \begin{bmatrix} \Delta\underline{u}_k^{(i)} \\ \Delta\underline{u}_A^{(i)} \\ \Delta\underline{u}_B^{(i)} \\ \Delta\underline{\lambda}_k^{(i)} \end{bmatrix}
$$

In the case of the sliding contact, the first term in Eq. (17) contributes to the vector ${}^{t+\Delta t}\underline{R}_c^{(i-1)}$, the second term yields a contribution to the tangent contact stiffness matrix ${}^{t+\Delta t}\underline{K}_c^{(i-1)}$ and the third term gives the overlap vector ${}^{t+\Delta t}\underline{\Delta}_c^{(i-1)}$ and contributes to ${}^{t+\Delta t}\underline{K}_c^{(i-1)}$. Hence, in this case, the tangent contact stiffness matrix contains the effects of a possible change in the location parameter $\beta^{(i-1)}$, which affects the elements of ${}^{t+\Delta t}\underline{K}_c^{(i-1)}$ corresponding to the incremental nodal point displacements. We now have

$$
{}^{t+\Delta t}\underline{R}_c^{(i-1)} = \begin{bmatrix} {}^{t+\Delta t}\lambda_{kx}^{(i-1)} \\ {}^{t+\Delta t}\lambda_{ky}^{(i-1)} \\ -(1-\beta^{(i-1)})\,{}^{t+\Delta t}\lambda_{kx}^{(i-1)} \\ -(1-\beta^{(i-1)})\,{}^{t+\Delta t}\lambda_{ky}^{(i-1)} \\ -\beta^{(i-1)}\ {}^{t+\Delta t}\lambda_{kx}^{(i-1)} \\ -\beta^{(i-1)}\ {}^{t+\Delta t}\lambda_{ky}^{(i-1)} \end{bmatrix} \qquad (22)
$$

$$
{}^{t+\Delta t}\underline{\Delta}_c^{(i-1)} = [-n_{sx}\ \Delta_{kx}^{(i-1)} - n_{sy}\ \Delta_{ky}^{(i-1)}] \qquad (23)
$$

$$
{}^{t+\Delta t}\underline{K}_{c}^{(i-1)} =
\begin{array}{|c|c|c|c|}
\hline
0 & 0 & -\bar{n}_{rx}{}^{t+\Delta t}\lambda_{kx}^{(i-1)} & -\bar{n}_{rx}{}^{t+\Delta t}\lambda_{ky}^{(i-1)} \\
\hline
 & 0 & -\bar{n}_{ry}{}^{t+\Delta t}\lambda_{kx}^{(i-1)} & -\bar{n}_{ry}{}^{t+\Delta t}\lambda_{ky}^{(i-1)} \\
\hline
 & & 2(1-\beta^{(i-1)})\bar{n}_{rx}{}^{t+\Delta t}\lambda_{kx}^{(i-1)} & (1-\beta^{(i-1)})\bar{n}_{rx}{}^{t+\Delta t}\lambda_{ky}^{(i-1)} \\
 & & & +(1-\beta^{(i-1)})\bar{n}_{ry}{}^{t+\Delta t}\lambda_{kx}^{(i-1)} \\
\hline
 & & & 2(1-\beta^{(i-1)})\bar{n}_{ry}{}^{t+\Delta t}\lambda_{ky}^{(i-1)} \\
\hline
\end{array}
$$

symmetric

$\bar{n}_{rx}^{t+\Delta t_{\lambda_{kx}}(i-1)}$	$\bar{n}_{rx}^{t+\Delta t_{\lambda_{ky}}(i-1)}$	$-n_{ry}$
$\bar{n}_{ry}^{t+\Delta t_{\lambda_{kx}}(i-1)}$	$\bar{n}_{ry}^{t+\Delta t_{\lambda_{ky}}(i-1)}$	n_{rx}
$-(1-\beta^{(i-1)})\,\bar{n}_{rx}^{t+\Delta t_{\lambda_{kx}}(i-1)}$ $+\beta^{(i-1)}\,\bar{n}_{rx}^{t+\Delta t_{\lambda_{kx}}(i-1)}$	$-(1-\beta^{(i-1)})\,\bar{n}_{rx}^{t+\Delta t_{\lambda_{ky}}(i-1)}$ $+\beta^{(i-1)}\,\bar{n}_{ry}^{t+\Delta t_{\lambda_{kx}}(i-1)}$	$(1-\beta^{(i-1)})\,n_{ry}$
$-(1-\beta^{(i-1)})\bar{n}_{ry}^{t+\Delta t_{\lambda_{kx}}(i-1)}$ $+\beta^{(i-1)}\,\bar{n}_{rx}^{t+\Delta t_{\lambda_{ky}}(i-1)}$	$-(1-\beta^{(i-1)})\,\bar{n}_{ry}^{t+\Delta t_{\lambda_{ky}}(i-1)}$ $+\beta^{(i-1)}\,\bar{n}_{ry}^{t+\Delta t_{\lambda_{ky}}(i-1)}$	$-(1-\beta^{(i-1)})\,n_{rx}$
$-2\beta^{(i-1)}\,\bar{n}_{rx}^{t+\Delta t_{\lambda_{kx}}(i-1)}$	$-\beta^{(i-1)}\,\bar{n}_{rx}^{t+\Delta t_{\lambda_{ky}}(i-1)}$ $-\beta^{(i-1)}\,\bar{n}_{ry}^{t+\Delta t_{\lambda_{kx}}(i-1)}$	$\beta^{(i-1)}\,n_{ry}$
	$-2\beta^{(i-1)}\,\bar{n}_{ry}^{t+\Delta t_{\lambda_{ky}}(i-1)}$	$-\beta^{(i-1)}\,n_{rx}$
		0

(24)

and the corresponding solution vector is

$$\begin{bmatrix} \Delta\underline{U}^{(i)} \\ \Delta\underline{\lambda}^{(i)} \end{bmatrix} = \begin{bmatrix} \Delta\underline{u}_k^{(i)} \\ \Delta\underline{u}_A^{(i)} \\ \Delta\underline{u}_B^{(i)} \\ \Delta\lambda_s^{(i)} \end{bmatrix}$$

Although we have simply listed the vectors ${}^{t+\Delta t}\underline{R}_c^{(i-1)}$ as shown in Eqs. (19) and (22), an important ingredient of our algorithm is that the actual elements of these force vectors are derived as explained in the next section.

Note that the above equations (used for the sample solutions in Section 4) correspond to a full Newton iteration. Our experiences with the solution of contact problems have so far shown that for the contact equations full Newton-Raphson iteration is usually best.

3. EVALUATION OF STICKING AND SLIDING CONDITIONS AND FRICTIONAL RESISTANCE

Much of the difficulty of solving contact problems lies in the design of appropriate procedures for numerically updating the contact conditions at a contactor node. In other words, the algorithm has to decide whether a node is not in contact and whether the matrices in Eqs. (19) to (21) for sticking contact or the matrices in Eqs. (22) to (24) for sliding contact shall be included in the system of equations. Appropriate decisions during the iteration concerning these conditions are most important for a reliable and effective scheme.

After iteration (i-1) the nodal point displacements ${}^{t+\Delta t}\underline{U}^{(i-1)}$ and nodal point forces $\Delta\underline{R}^{(i-1)}$ are known where (see Fig. 4)

$$\Delta\underline{R}^{(i-1)} = {}^{t+\Delta t}\underline{R} - {}^{t+\Delta t}\underline{F}^{(i-1)} \quad . \tag{25}$$

We note that at the nodes not belonging to a contact surface the components of $\Delta\underline{R}^{(i-1)}$ are the out-of-balance loads usually encountered in nonlinear analysis [16], but corresponding to the boundary nodes affected by the contact, the contact forces ${}^{t+\Delta t}\underline{R}_c^{(i-1)}$ are active. These forces are evaluated from the out-of-balance $\Delta\underline{R}^{(i-1)}$ and correspond to tension release, sticking or sliding conditions.

The procedure of calculating the contact forces from the vector $\Delta\underline{R}^{(i-1)}$ is effective because an incrementation of the Lagrange multipliers used in Eq. (18) can – in other than geometrically and materially linear analyses of sticking contact conditions – lead to serious errors of linearization.

In the following we consider the contactor segments and contactor nodes, and we discuss how the conditions of node sticking and sliding can be reached, and how the contact forces ${}^{t+\Delta t}\underline{R}_c^{(i-1)}$ are evaluated.

When a contactor node penetrates the target body in an iteration, which is decided kinematically by the displacements of the contactor and target bodies leading to a geometric overlap (see Fig. 3), the matrices in Eqs. (19) to (21) are included in the solution for the next incremental displacements. Hence, in the first iteration from no contact to a contact condition, sticking is assumed.(+) This is the mechanism used to evaluate the nodal point forces and enable a decision on whether sticking or sliding conditions are really applicable.

3.1 Contactor Segment Distributed Tractions and Resultant Forces

The decision on whether a contactor node is releasing or is in sticking or sliding conditions is perhaps most quickly based on considering the total and relative magnitudes of the calculated nodal points forces. However, this can lead to some numerical difficulties, and it is deemed more effective to establish the condition at a contactor node from the accumulated effects and conditions of the contactor segments adjacent to the node.

The first step in our procedure is to calculate the distribution of the tractions along the contactor boundary given the nodal point reactions $\Delta\underline{R}^{(i-1)}$. Let t_x^k and t_y^k be the magnitudes of the distributed tractions (force/unit area) at the nodal point k (see Fig. 4), then we have with a linear displacement interpolation in a "consistent" approach to calculate the tractions from the nodal point forces, in plane stress

(+) We may note that for the special case of frictionless contact, i.e. $\mu_s = \mu_d = 0.0$, we can directly assume perfect sliding conditions.

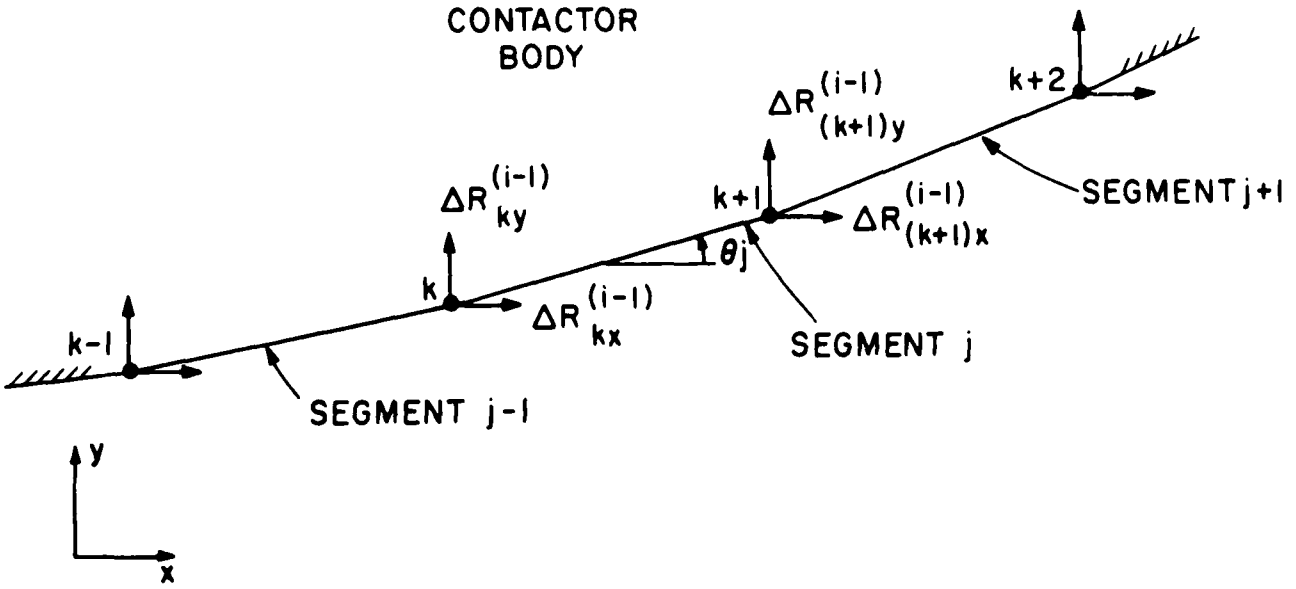

a) Out-of-balance forces acting onto contactor body

Figure 4. Calculation of normal and tangential tractions onto contractor body

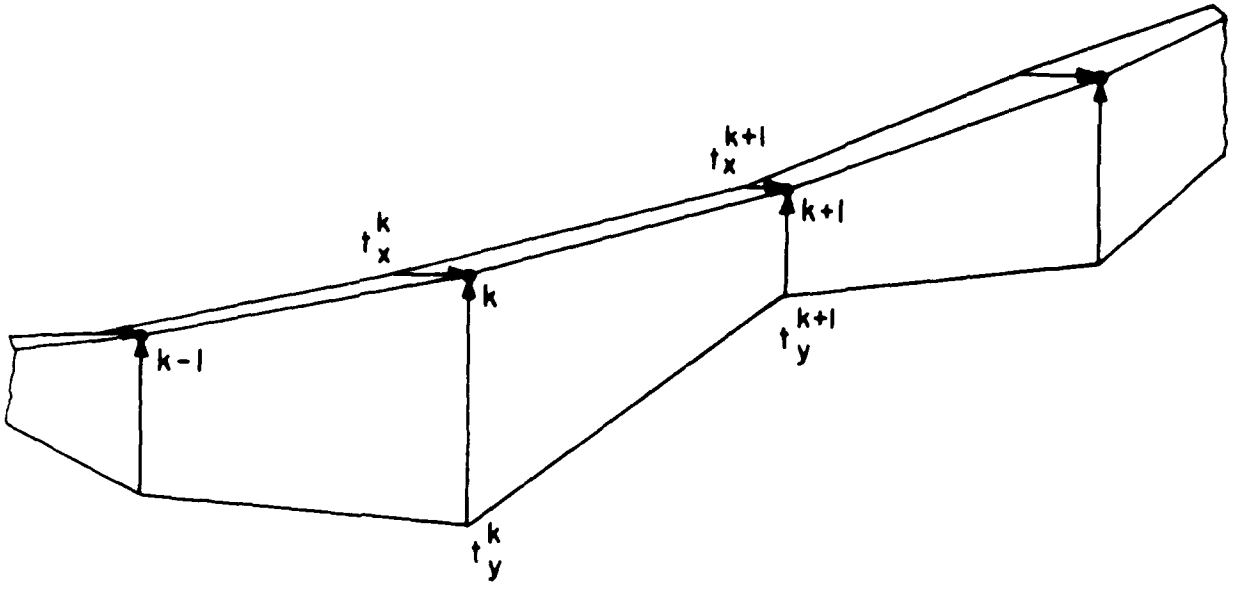

b) Tractions acting onto contactor body

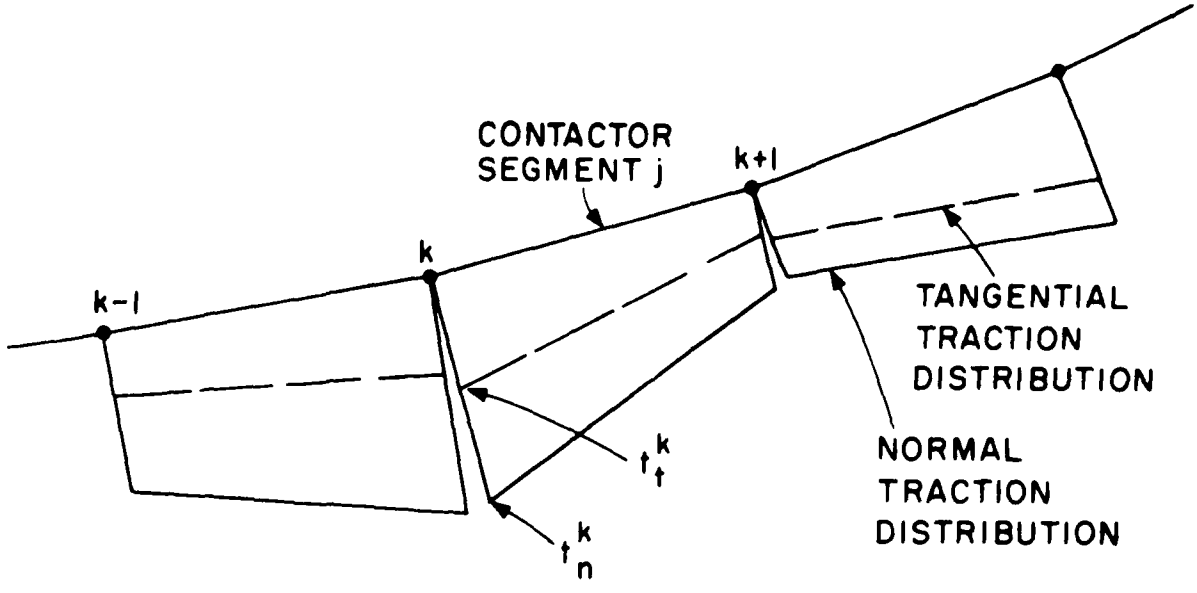

c) Normal and tangential tractions onto contactor body. Normal traction is positive when acting onto the body, tangential traction is positive when acting from node k to node (k+1).

Figure 4 Calculation of normal and tangential tractions onto contactor body.

and plane strain analyses, with uniform thickness h,[+]

$$\begin{bmatrix} \Delta R_{kx}^{(i-1)} \\ \Delta R_{ky}^{(i-1)} \end{bmatrix} = h \begin{bmatrix} t_x^{k-1} & t_x^{k} & t_x^{k+1} \\ t_y^{k-1} & t_y^{k} & t_y^{k+1} \end{bmatrix} \begin{bmatrix} \frac{d_{j-1}^{(i-1)}}{6} \\ \frac{d_{j-1}^{(i-1)} + d_j^{(i-1)}}{3} \\ \frac{d_j^{(i-1)}}{6} \end{bmatrix} \quad (26)$$

and in axisymmetric analysis (assuming the y-axis to be the axis of revolution)

$$\begin{bmatrix} \Delta R_{kx}^{(i-1)} \\ \Delta R_{ky}^{(i-1)} \end{bmatrix} = \begin{bmatrix} t_x^{k-1} & t_x^{k} & t_x^{k+1} \\ t_y^{k-1} & t_y^{k} & t_y^{k+1} \end{bmatrix} \begin{bmatrix} \frac{d_{j-1}^{(i-1)}}{12} \left({}^{t+\Delta t}x_{k-1}^{(i-1)} + {}^{t+\Delta t}x_{k}^{(i-1)} \right) \\ \frac{d_{j-1}^{(i-1)}}{12} \left({}^{t+\Delta t}x_{k-1}^{(i-1)} + 3\ {}^{t+\Delta t}x_{k}^{(i-1)} \right) + \frac{d_j^{(i-1)}}{12} \left(3\ {}^{t+\Delta t}x_{k}^{(i-1)} + {}^{t+\Delta t}x_{k+1}^{(i-1)} \right) \\ \frac{d_j^{(i-1)}}{12} \left({}^{t+\Delta t}x_{k}^{(i-1)} + {}^{t+\Delta t}x_{k+1}^{(i-1)} \right) \end{bmatrix} \quad (27)$$

[+] Instead of using the consistent traction recovery given here, it would also be possible to employ a lumped approach.

where ${}^{t+\Delta t}x_k^{(i-1)}$ is the x-coordinate of nodal point k at the end of iteration (i-1). Using Eqs. (26) and (27) a tridiagonal coefficient matrix is established that relates the unknown tractions to the known values of $\Delta\underline{R}^{(i-1)}$, and the equations can be solved to calculate, in each iteration, the nodal values t_x^k and t_y^k for all nodes in contact. These values are then employed to evaluate the tangential and normal segment tractions, t_t^k and t_n^k, at the nodes. Note that to evaluate these tractions for segment j, the values t_x^k, t_y^k and t_x^{k+1}, t_y^{k+1} are simply transformed to the tangential and normal directions defined by the angle θ_j of the segment. This results in general into a discontinuity of the normal and tangential segment tractions at the nodal points, see Fig. 4.

For the definition of the state of a segment, we need the total normal and tangential forces applied to the segment. In the case of plane stress and plane strain analyses, the total resultant normal force, T_n^j, acting on segment j is

$$T_n^j = h \frac{d_j^{(i-1)}}{2} (t_n^k + t_n^{k+1}), \tag{28}$$

and the total resultant tangential force, T_t^j, acting on segment j is

$$T_t^j = h \frac{d_j^{(i-1)}}{2} (t_t^k + t_t^{k+1}), \tag{29}$$

where $d_j^{(i-1)}$ is the length of the contactor segment j in iteration (i). Similarly, for axisymmetric analysis we have

$$T_n^j = \frac{d_j^{(i-1)}}{6} \Big\{ 2 \left({}^{t+\Delta t}x_k^{(i-1)}\, t_n^k + {}^{t+\Delta t}x_{k+1}^{(i-1)}\, t_n^{k+1} \right) + \left({}^{t+\Delta t}x_{k+1}^{(i-1)}\, t_n^k + {}^{t+\Delta t}x_k^{(i-1)}\, t_n^{k+1} \right) \tag{30}$$

and

$$T_t^j = \frac{d_j^{(i-1)}}{6} 2 \left({}^{t+\Delta t}x_k^{(i-1)} \, t_t^k + {}^{t+\Delta t}x_{k+1}^{(i-1)} \, t_t^{k+1} \right) + \left({}^{t+\Delta t}x_{k+1}^{(i-1)} \, t_t^k + {}^{t+\Delta t}x_k^{(i-1)} \, t_t^{k+1} \right) . \quad (31)$$

With the above calculations completed the algorithm decides on the state of the segment using the segment resultant forces T_n^j, T_t^j and Coulomb's law of friction globally applied over the segment.

3.2 Segment Release

The segment is assumed to have experienced tension release if T_n^j is negative, and in this case the contactor segment normal and tangential tractions are set to zero.

3.3 Assume Segment was in Previous Iteration in Sticking Contact

Using the total normal force on the segment T_n^j the frictional capacity of the segment T_f^j is calculated using Coulomb's law of friction, $T_f^j = \mu_s T_n^j$, where μ_s for the segment is set equal to μ_d if the segment was ever in sliding (see Section 4.2). The following two situations can now arise.

Case 1: The frictional capacity of the segment is larger than the applied total tangential force, i.e., $T_f^j \geq |T_t^j|$. The segment continues to stick.

Case 2: The frictional capacity of the segment is smaller than the applied total tangential force, i.e., $T_f^j < |T_t^j|$. The state of the segment is now updated to sliding, with $T_f^j = \mu_d T_n^j$.

The results on whether the segment continues to stick or is now sliding are later used in deciding whether the contactor nodes are sticking or sliding (see Section 3.5).

Aside from deciding on the sticking and sliding conditions of the segments, also the contributions to the vector ${}^{t+\Delta t}\underline{R}_c^{(i-1)}$ must be evaluated. This is done differently in the above two situations.

In case 1 the distributed tangential and normal tractions on the segment j are employed to calculate the nodal point consistent loads, see Fig. 5. We note that if also the conditions of the adjacent segments (j-1) and (j+1) correspond to case 1, these nodal point consistent loads are at the nodes k and k+1 simply minus the values in $\underline{R}^{(i)}$.

In case 2 the segment is sliding, and Fig. 5(b) summarizes the tractions t_t used in the calculation of ${}^{t+\Delta t}\underline{R}_c^{(i-1)}$. Note that a uniform traction is assigned such that in sliding conditions the total tangential force is scaled down to equal the frictional capacity. Using a uniform frictional traction represents perhaps the simplest way of globally satisfying Coulomb's law of friction over the segment.(±) Figure 5 shows the tractions used in plane stress and plain strain analyses; in axisymmetric solution the value $(t_t^k + t_t^{k+1})/2$ of Fig. 5 is replaced by $\tilde{t}_t$,

$$\tilde{t}_t = \frac{2\, T_t^j}{d_j^{(i-1)}\,({}^{t+\Delta t}x_k^{(i-1)} + {}^{t+\Delta t}x_{k+1}^{(i-1)})} \quad . \qquad (32)$$

In summary, unless there is tension release (see Section 3.2) the contact forces ${}^{t+\Delta t}\underline{R}_c^{(i-1)}$ are calculated as the consistent nodal point loads corresponding to the tangential tractions t_t, shown in Fig. 5, and the unaltered normal tractions shown in Fig. 4. In tension release both the normal and tangential tractions on the segment are set to zero.

3.4 Assume Segment was in Previous Iteration in Sliding Contact

If the segment was in sliding contact, analogous calculations to those described in Section 3.3 are performed, but the friction coefficient used is μ_d. Hence, in case 1 the segment changes to sticking, whereas in case 2 the segment continues to slide.

3.5 Conditions of Contactor Nodes

Once the conditions of the contactor segments have been decided

(±) Updating the tangential tractions in this way raises questions on the convergence of the iterative solution as studied in a forthcomning communication.

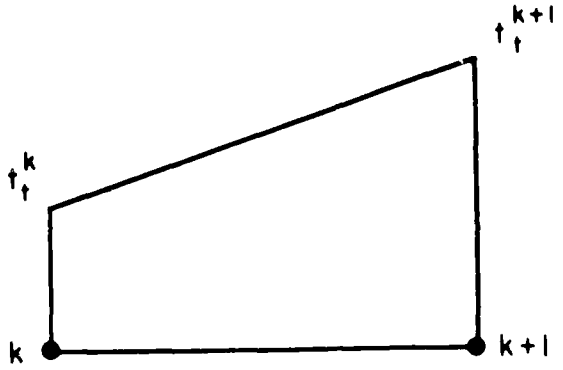

a) Case 1

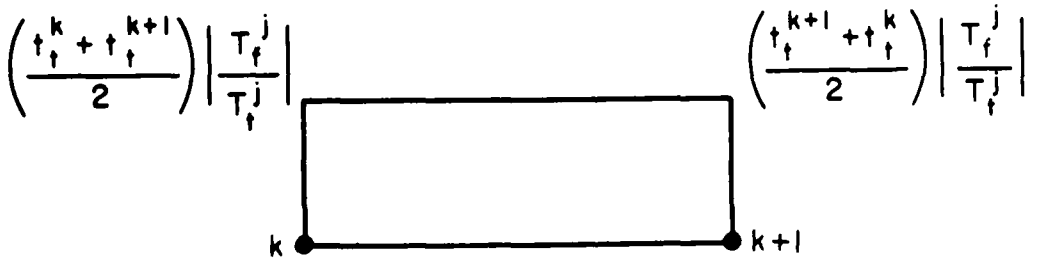

b) Case 2

Figure 5 Tangential tractions used in calculation of contact force vector $t+\Delta t_{\underline{R}_c}(i-1)$; in axisymmetric analysis replace $(t_t^k + t_t^{k+1}) / 2$ by $\tilde{t}_t$ of Eq. (32).

as discussed above, the algorithm determines the conditions of the nodes on the contactor surface. Table 1 summarizes how the various conditions (release, sticking and sliding) of a contactor node are reached. We may note that these conditions decide on whether zero (corresponding to no contact or contact release), one (corresponding to sliding) or two (corresponding to sticking) contact equations are to be included in the incremental equations for each contactor node.

The decision on whether a contactor node k is not in contact, or is in sliding or sticking contact, and the evaluation of the contact matrices (in Eqs. (21) and (24)) and the contact forces to be used in Eq. (18) gives all the ingredients to proceed with the iteration (i).

4. SOME SAMPLE SOLUTIONS

The algorithm presented in the previous sections was implemented in ADINA and in the following we present the results of some sample analyses. In these analyses, the primary objective was to study the performance of the algorithm in order to identify where improvements are needed rather than to solve actual practical problems.

It is our experience that regarding the solution of contact problems some "very simple looking" problems, including frictional conditions and the elasticity of the structure, may provide quite severe tests on the performance of an algorithm, and in fact may be more difficult to solve than actual practical engineering problems.

4.1 Analyses of Hertz Contact Problems

Figure 6 shows the contact problem considered and the finite element idealization used. In this problem a long cylinder with radius R=10 was analyzed; hence in the model plane, strain conditions were assumed. The rigid target surface was modeled by specifying nodes with no degrees of freedom. In the region of anticipated contact, 8-node elements were used to model the contactor with one contactor segment always spanning over one 8-node element side, and these elements were modeled as materially-nonlinear-only or using the total Lagrangian formulation [16]. To simulate the load application, the vertical displacements were prescribed along the top surface of the model and the total load P for a prescribed displacement was calculated by integrating the contact pressures. Figure 7 gives the calculated contact pressures and a comparison with the Hertz analytical solution [21].

We may note that only a few solution points are given in Fig. 7, because the program outputs the mean traction over a segment and at the maximum applied load (P = 6600) only three segments were in

TABLE 1. STATE OF CONTACTOR NODE AS DECIDED BY STATES OF ADJOINING SEGMENTS

STATE OF ADJOINING SEGMENTS		STATE OF NODE
one adjoining segment	other adjoining segment	
sticking	sticking sliding tension release	sticking
sliding	sliding tension release	sliding
tension release	tension release	tension release

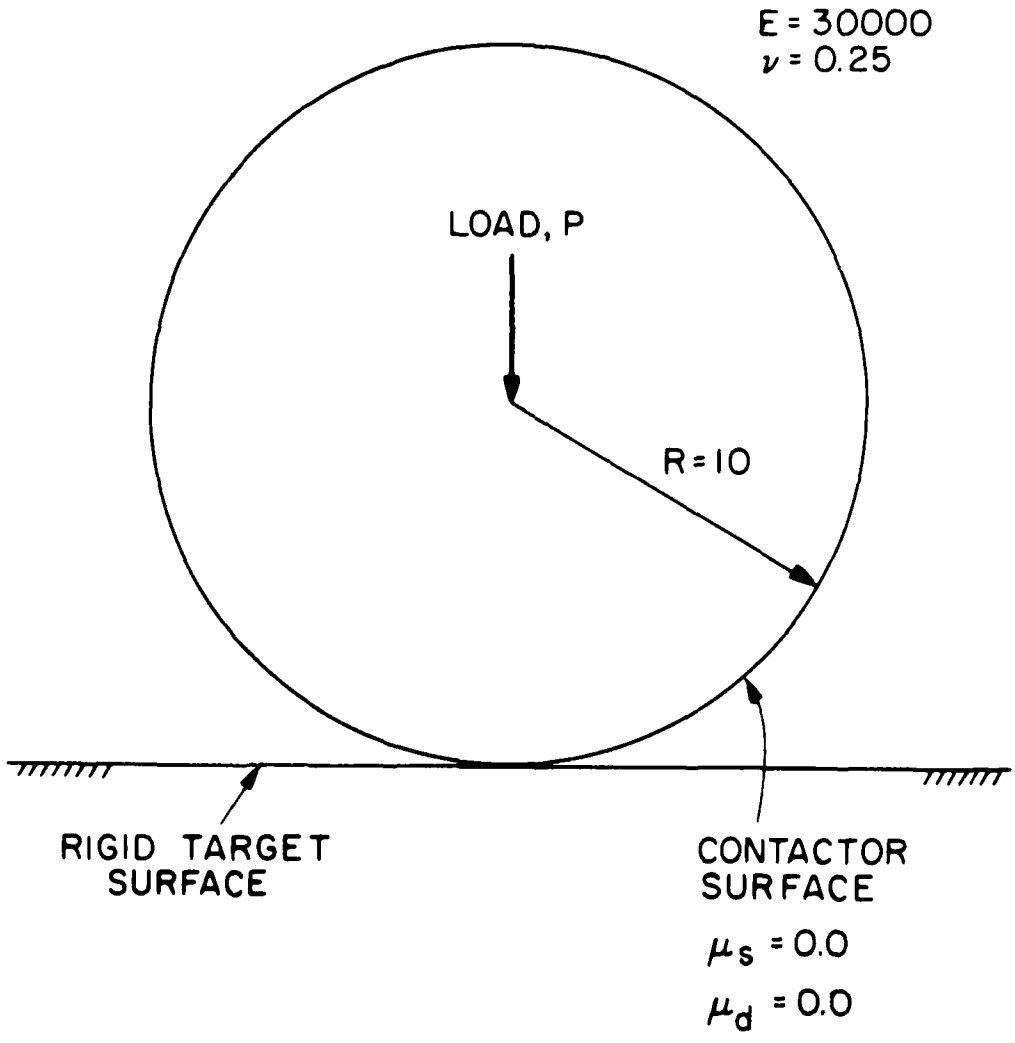

a) Problem considered

Figure 6. Analysis of Hertz plane strain contact problem (M.N.O. and T.L. formulations denote materially-nonlinear-only and total Lagrangian formulations, resp. [16])

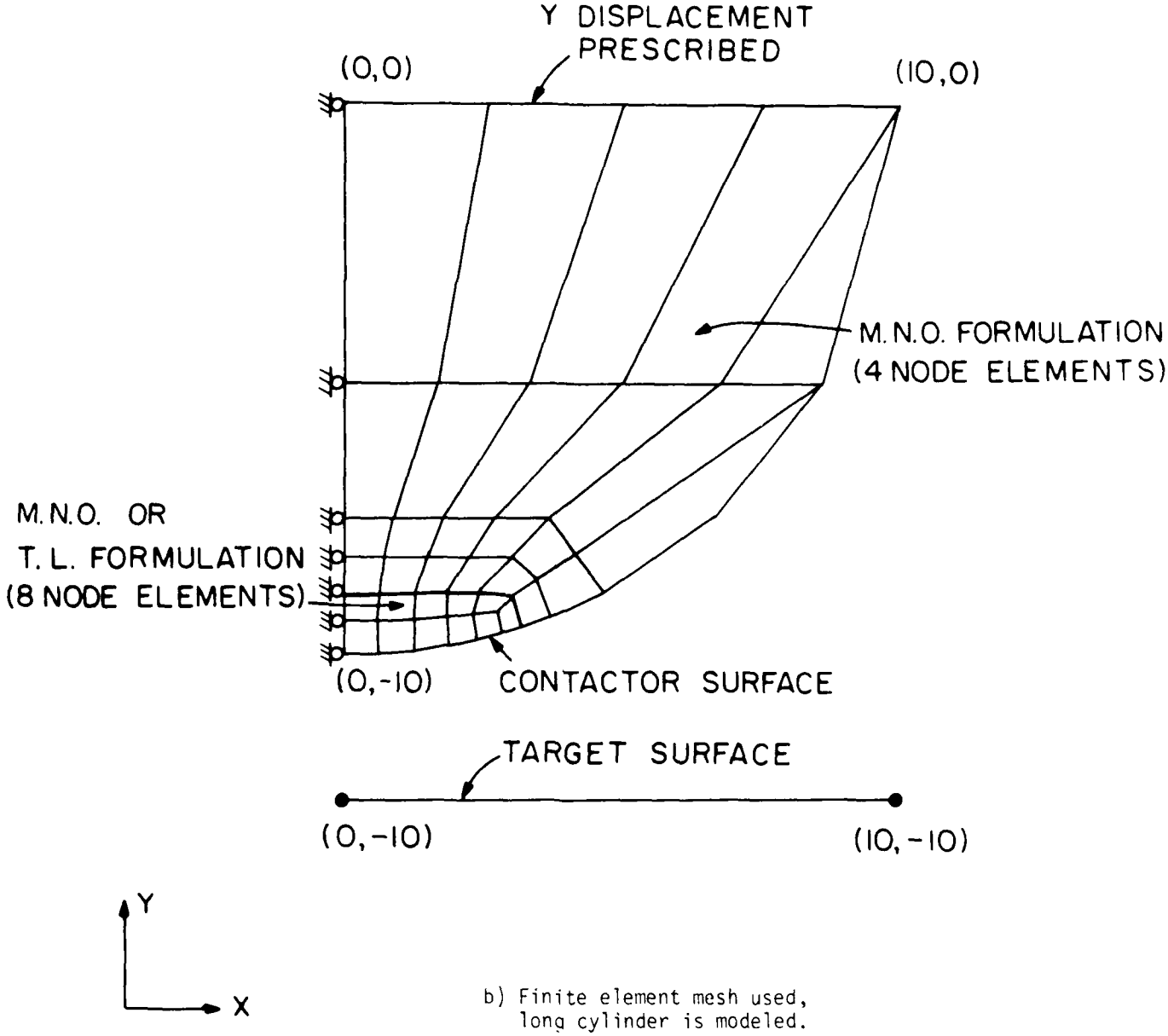

b) Finite element mesh used, long cylinder is modeled.

Figure 6 Analysis of Hertz plane strain contact problem (M.N.O. and T.L. formulations denote materially-nonlinear-only and total Lagrangian formulations, resp. [16])

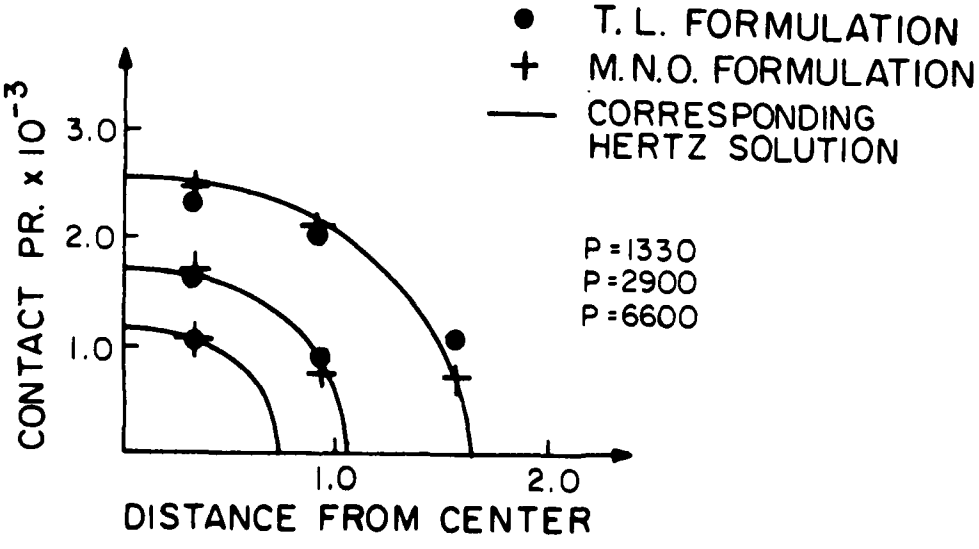

Figure 7 Solution to the plane strain Hertz problem

contact. In order to obtain more finite element solution points and a higher solution accuracy, a finer finite element discretization on the contactor surface is required.

Next, the Hertz contact problem of a sphere of radius R=100 was analyzed. Hence, Fig. 6 (a) still shows the contact problem, but now R=100.0 and axisymmetric conditions are considered. Figure 8 gives the finite element mesh used in this analysis and, Fig. 9 shows the calculated contact pressures and a comparison with the Hertz solution.

4.2 Motion of a Rubber Sheet in a Converging Channel

A sheet of rubber in plane stress was confined to move in a rigid horizontal channel. Figure 10 shows the sheet and the finite element idealization used.(+) The right face of the sheet was subjected to the displacement history given in Fig. 11, making this a large deformation problem. Note that the displacements were assumed to vary slowly so that inertia effects could be neglected.

Although the solution obtained could not be compared with an available solution, this is an interesting problem to study the performance of the contact algorithm. Also, the essential features and solution difficulties of this problem are frequently encountered in actual practical problems; e.g., analysis of metal forming processes.

Figure 12 shows the distribution of normal and tangential tractions for different load steps in the solution. The tractions close to the face at which the displacements are imposed are not shown because a fine finite element idealization would be required to obtain good stress predictions near the face. Note that the magnitudes of the tangential tractions, t_t, for times 8, 14 and 24 are essentially equal to μ_d times t_n — because practically the entire rubber sheet is sliding through the channel — and that the tangential tractions at time 24 are acting in the opposite direction to the tractions at times 8 and 14. However, at time 18 the tangential tractions have only partially reversed and some segments are still in sticking conditions. It is this change in tangential tractions, resulting from the reversal in motion, that is quite difficult to analyze.

Figure 12 also shows the results obtained when assuming a frictionless motion. As expected, for the frictionless case the normal tractions are significantly larger at times 8 and 14 (the imposed displacements increase) and smaller at times 18 and 24 (the imposed displacements decrease), when compared with the results including friction.

(+) Note that the rigid target surface was modeled using 12 segments for the sole purpose of demonstrating that contactor nodes can slide over target nodes.

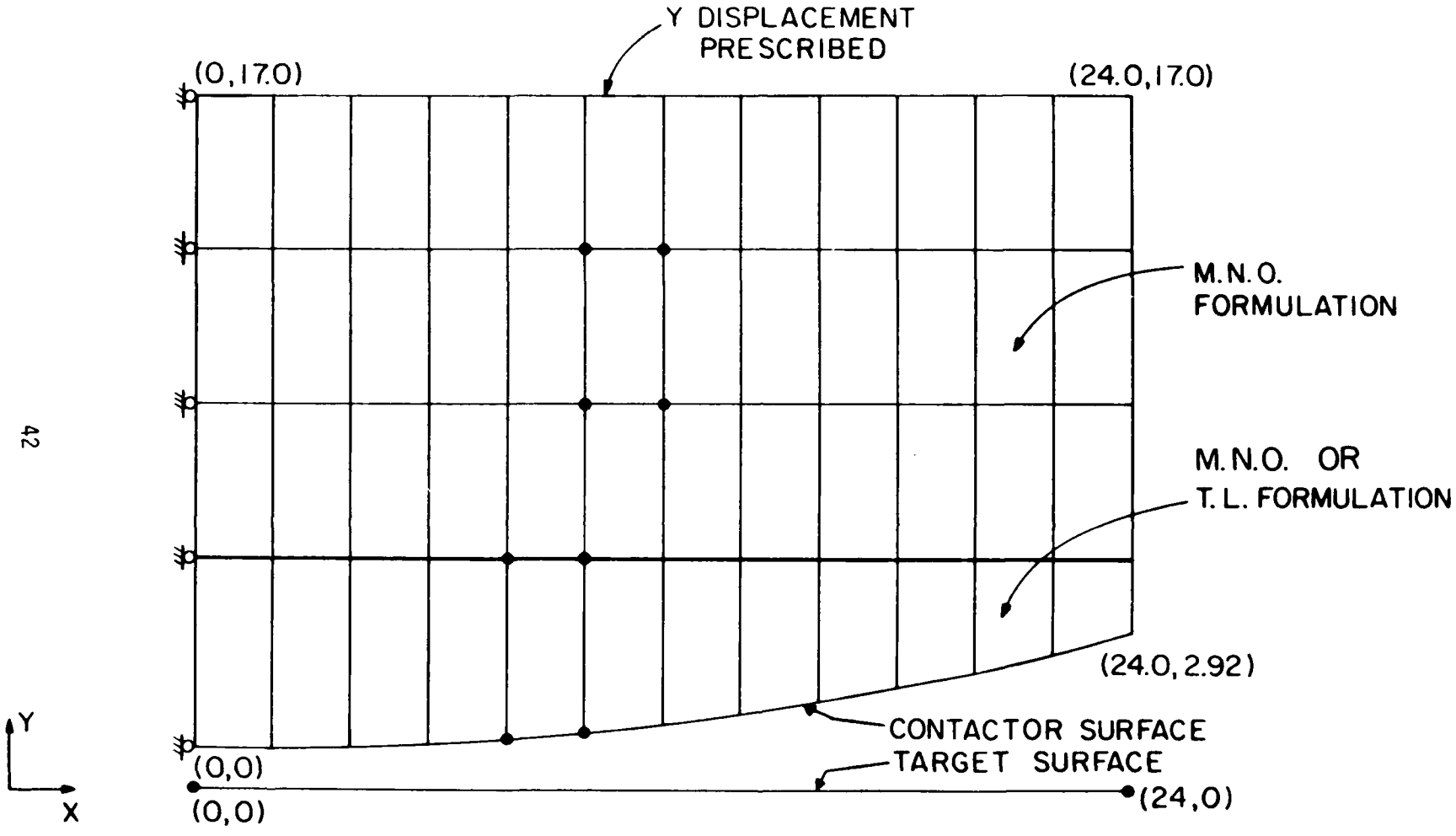

Figure 8 Analysis of Hertz axisymmetric contact problem

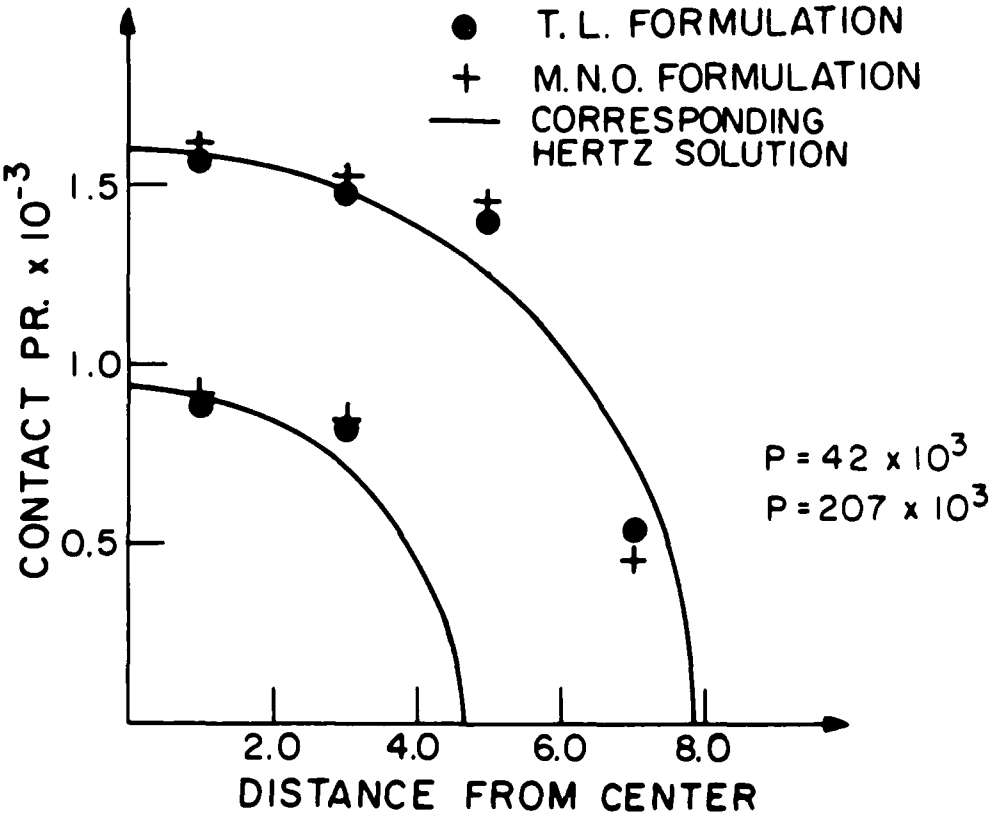

Figure 9 Solution to the axisymmetric Hertz problem

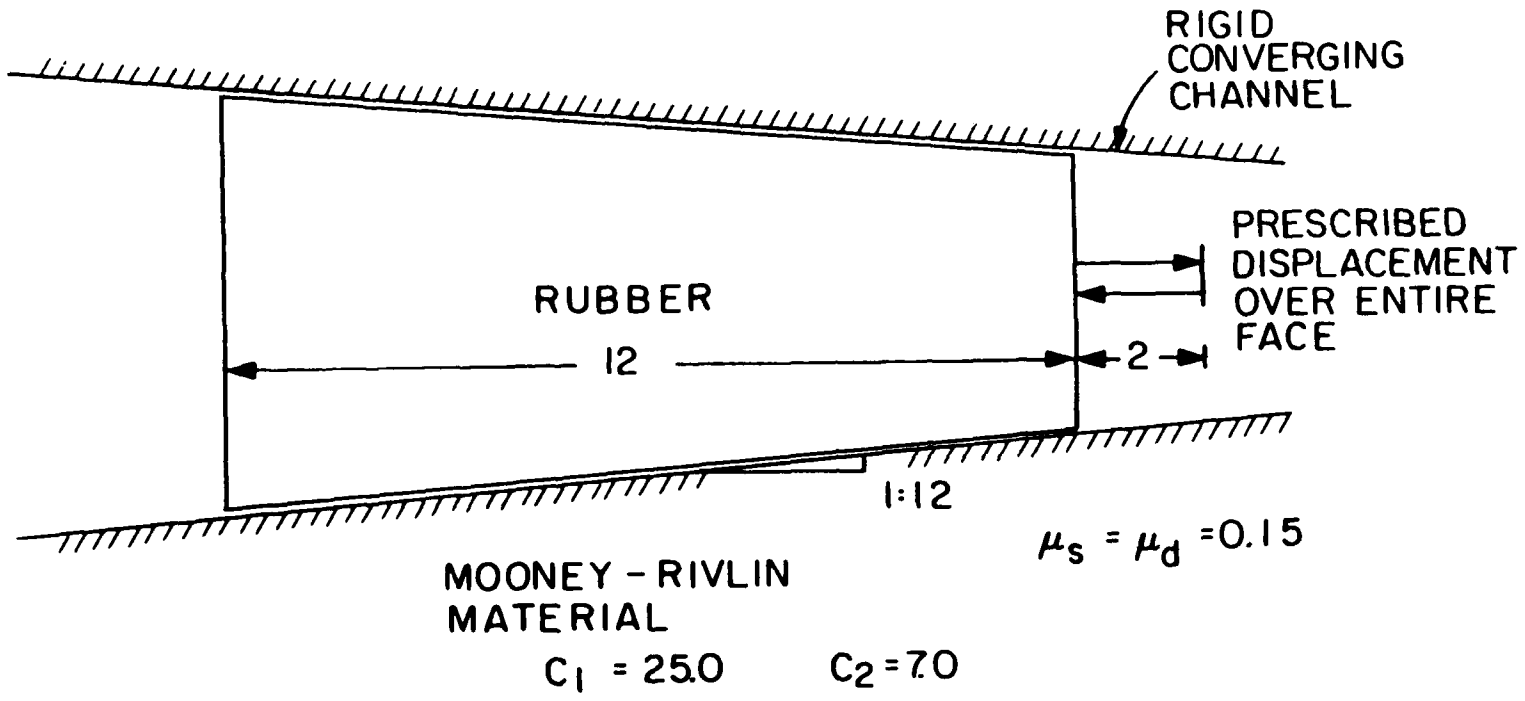

a) Problem considered

Figure 10. Analysis of motion of a rubber sheet in a converging channel

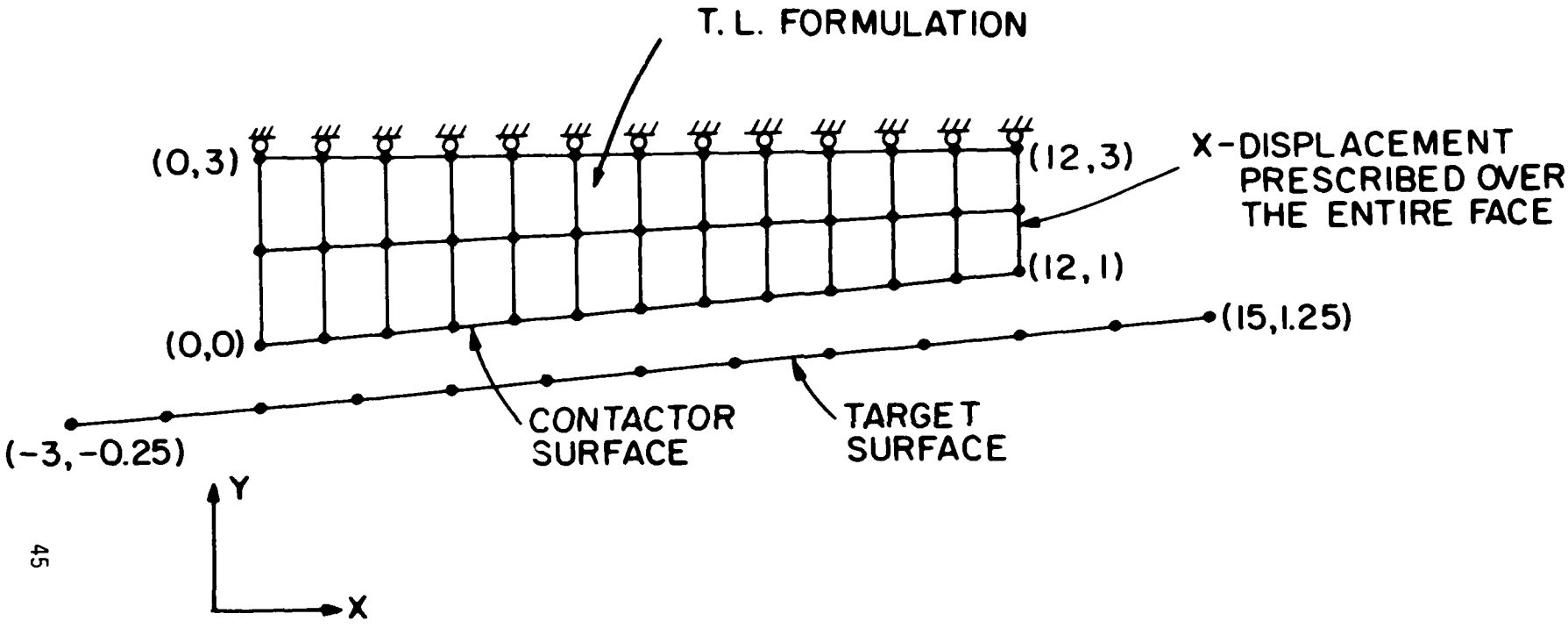

b) Finite element mesh used

Figure 10 Analysis of motion of a rubber sheet in a converging channel

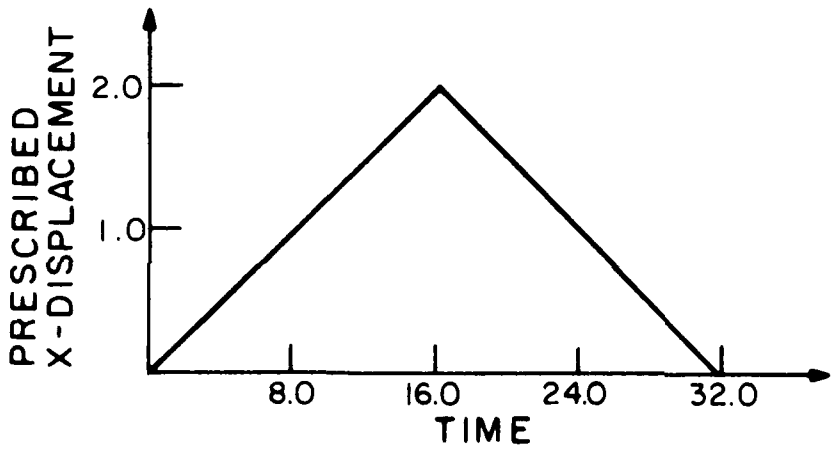

Fig. 11 Prescribed displacements in analysis of rubber sheet, time step $\Delta t = 0.5$

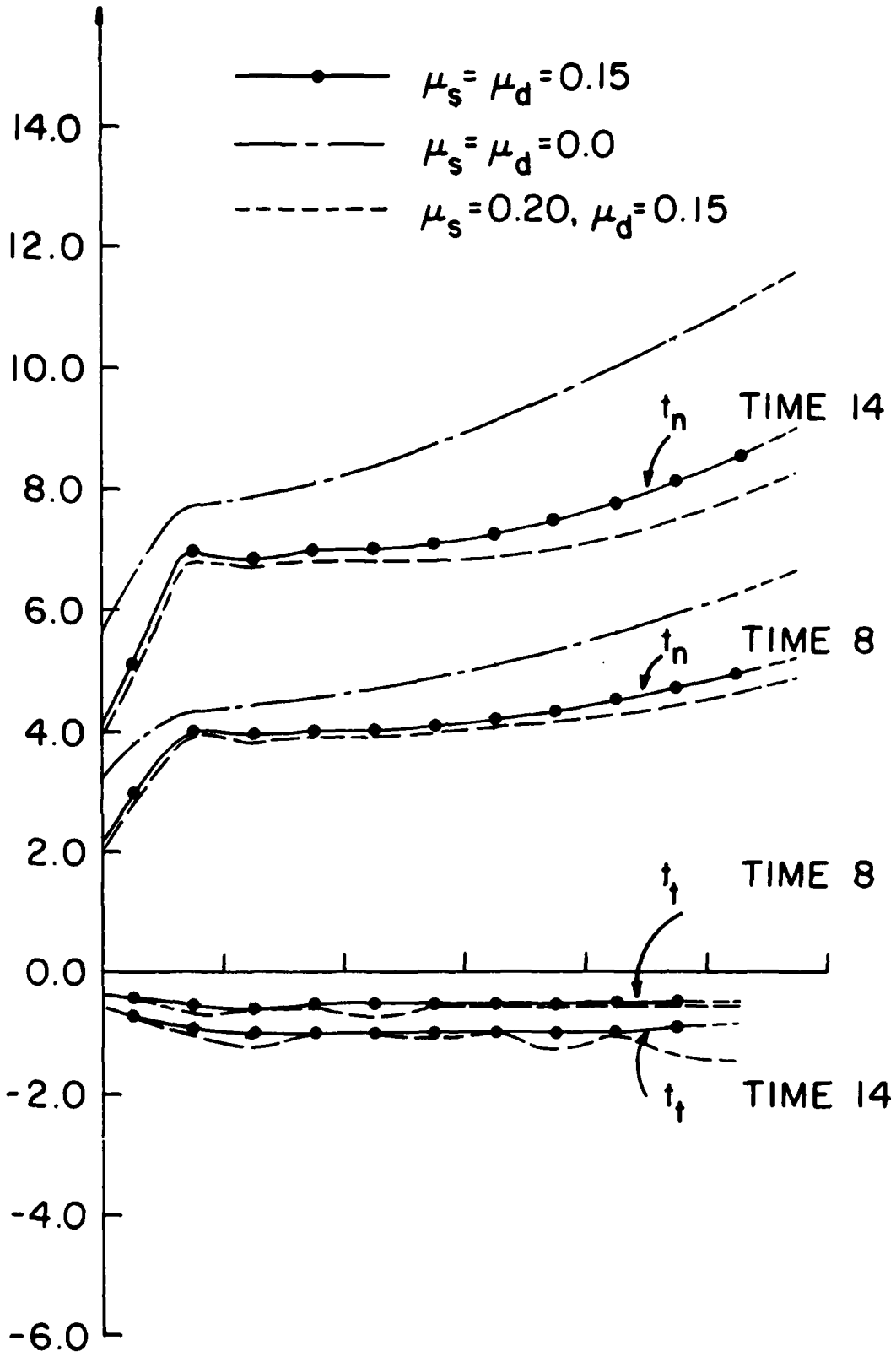

a) At times 8 and 14

Figure 12 Distributed tractions in analysis of rubber sheet moving through rigid channel. (Solid line refers to the solution for $\mu_s = \mu_d$ and the solution for $\mu_s > \mu_d$ using our usual algorithm; dashed line refers to "experiment" when $\mu_s > \mu_d$)

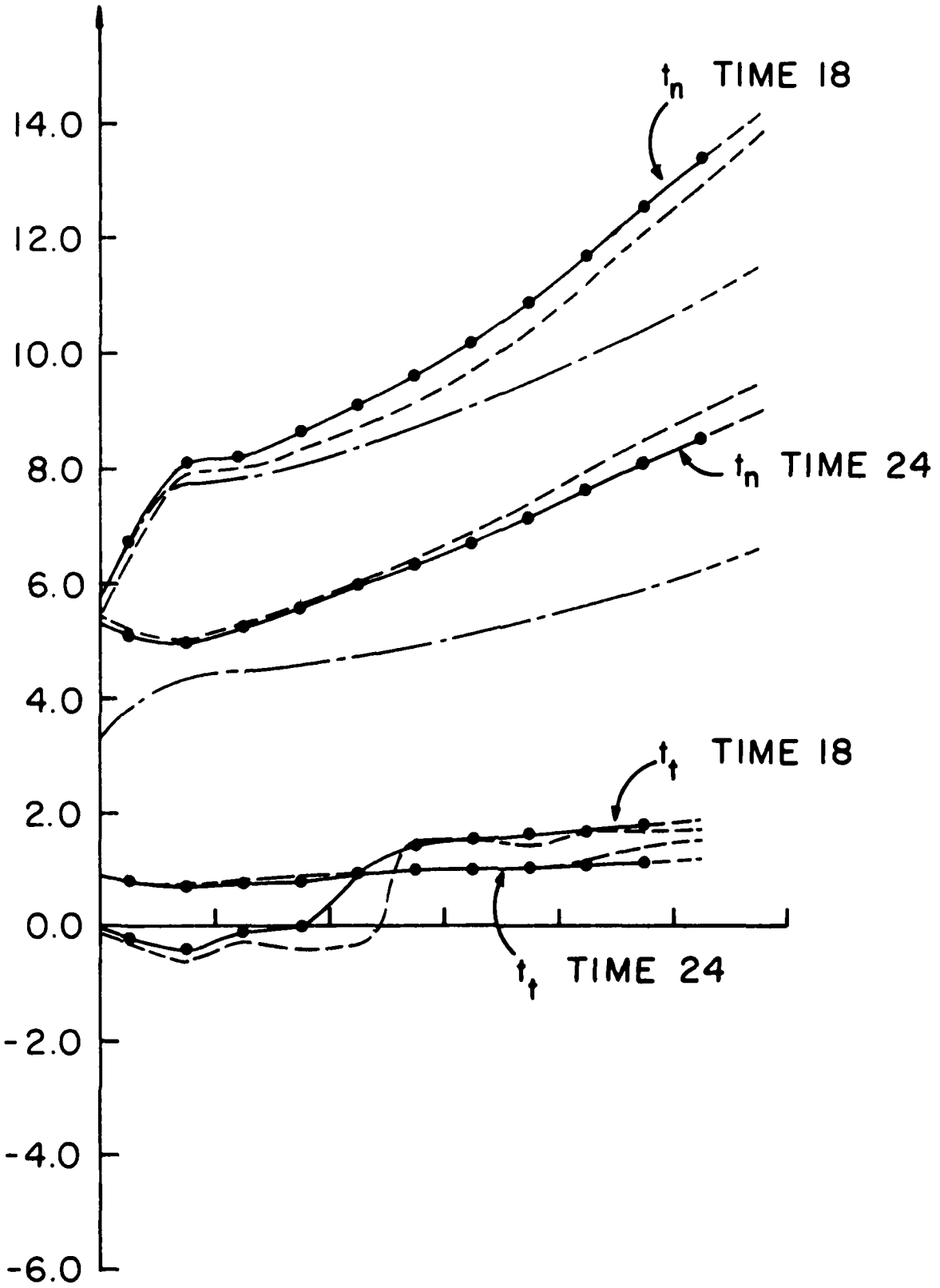

b) At times 18 and 24

Figure 12 continued

Finally, the motion of the rubber sheet for $\mu_s > \mu_d$ was also analyzed ($\mu_s = 0.20$, $\mu_d = 0.15$). For this case, two different solution algorithms were employed. In the first solution our usual algorithm was used, in which the value of μ_s for a segment was set equal to μ_d as soon as, and for all times thereafter, the static frictional resistance was exceeded for the segment. Since the effect of $\mu_s > \mu_d$ is then a transient phenomenon, the solution results for the times considered in Fig. 12 are (very closely) the same as the results obtained for the case $\mu_s = \mu_d$. In the second analysis, as an experiment, the value of $\mu_s = 0.20$ was kept throughout the solution and the results marked $\mu_s = 0.20$, $\mu_d = 0.15$ in Fig. 12 were obtained. It should be noted that in this analysis the time step ($\Delta t = 0.5$) is an important (physical) variable of the problem — because the solution procedure simulates the frictional motion of the sheet for each solution step separately — and it is questionable whether the assumptions used in this numerical solution appropriately simulate the actual physical process of motion. However, it is interesting to note that for the chosen values of μ_s and μ_d relatively small differences in the tractions were calculated when compared with the solution for $\mu_s = \mu_d$ (except for the tangential tractions at time 18 which more drastically changed sign when $\mu_s > \mu_d$). It should be emphasized that these solutions of the rubber sheet when $\mu_s > \mu_d$ should only be regarded as a rather brief numerical experiment, because there are many difficult questions related to the physics and to our numerical analysis procedure for this problem that need much further study [19].

4.3 Analysis of a Snapped Wire in Continuous Writing

The practical application of this problem lies in the analysis of the conditions that arise when a wire of a continous wiring around a cylinder snaps.

Figure 13 shows the model considered. Note that the snapped wire is free of constraints at $x = 0$ (for $y \geq 0$). The objective was to calculate the stress distribution in the continuous wiring (modeled here as a continuum at the maximum load application, $\sigma_{yy} = 300$ MPa and $\sigma_{xx} = 750$ MPa.

Figure 13 (b) shows the finite element idealization used for the analysis in Fig. 14 gives some calculated stresses and a comparison with the results obtained by Boman [22]. The solution with our contact

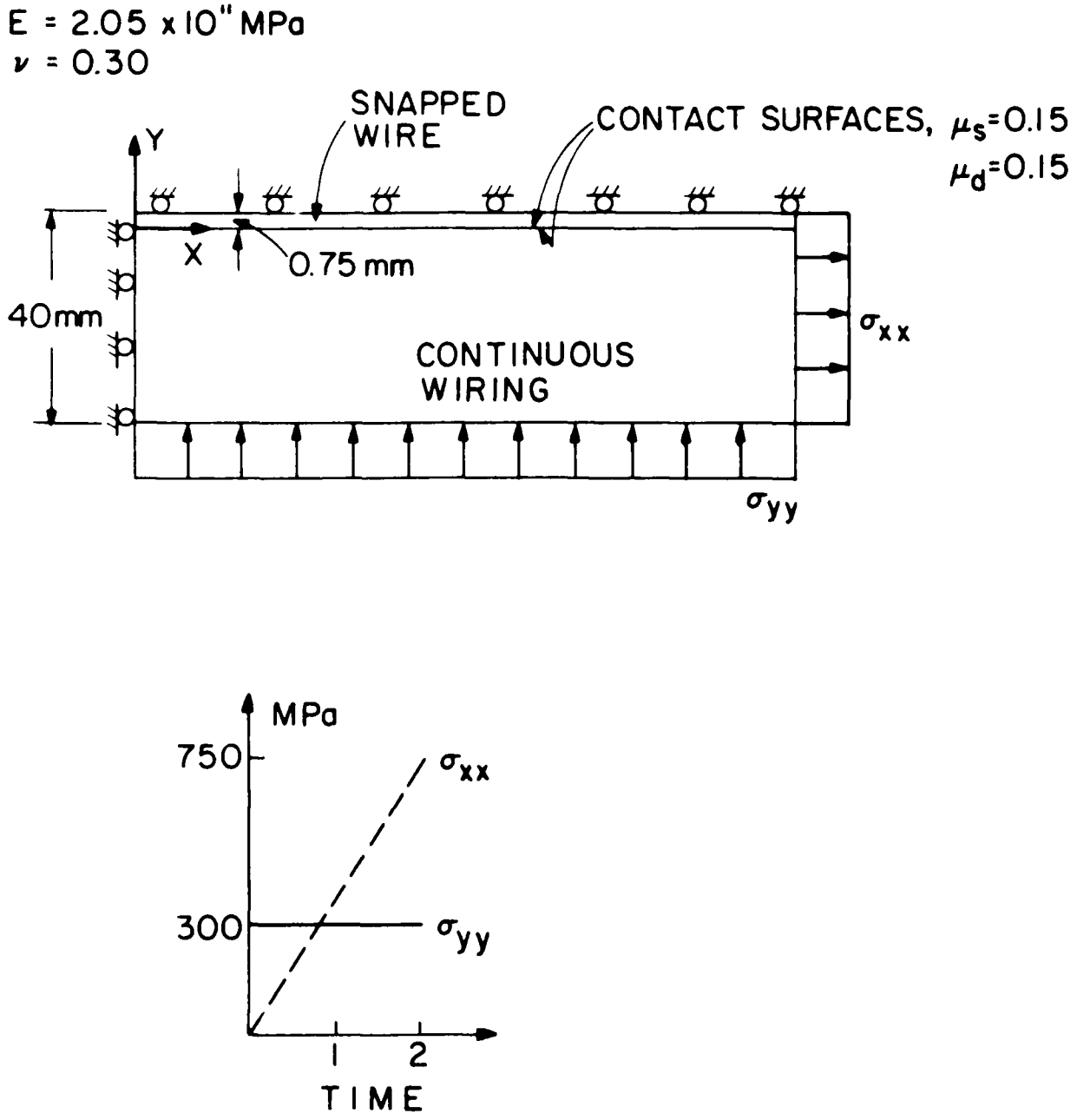

a) Problem considered , time step $\Delta t = 1.0$

Figure 13. Analysis of wiring around cylinder

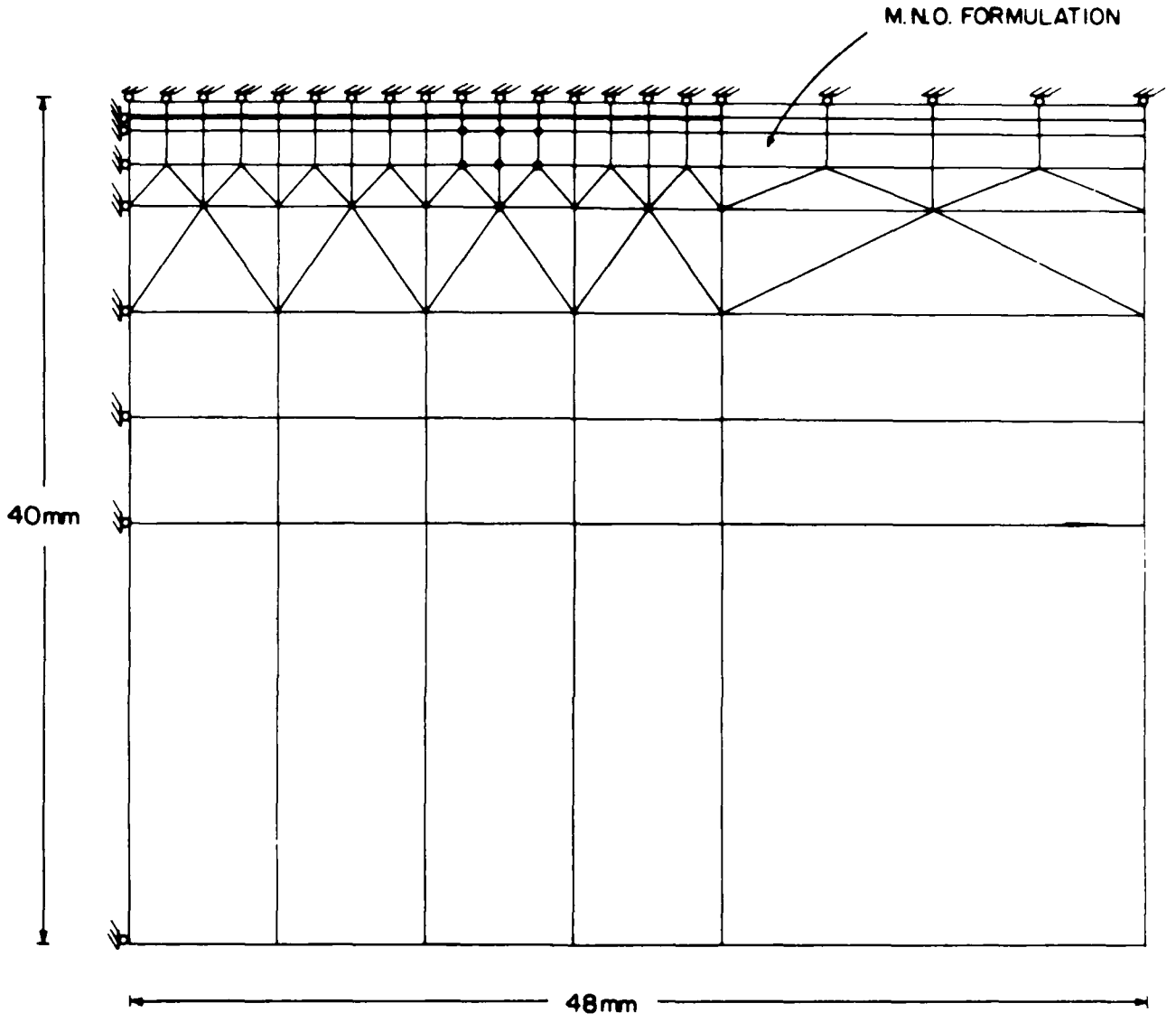

b) Finite element mesh used

Figure 13 Analysis of wiring around cylinder

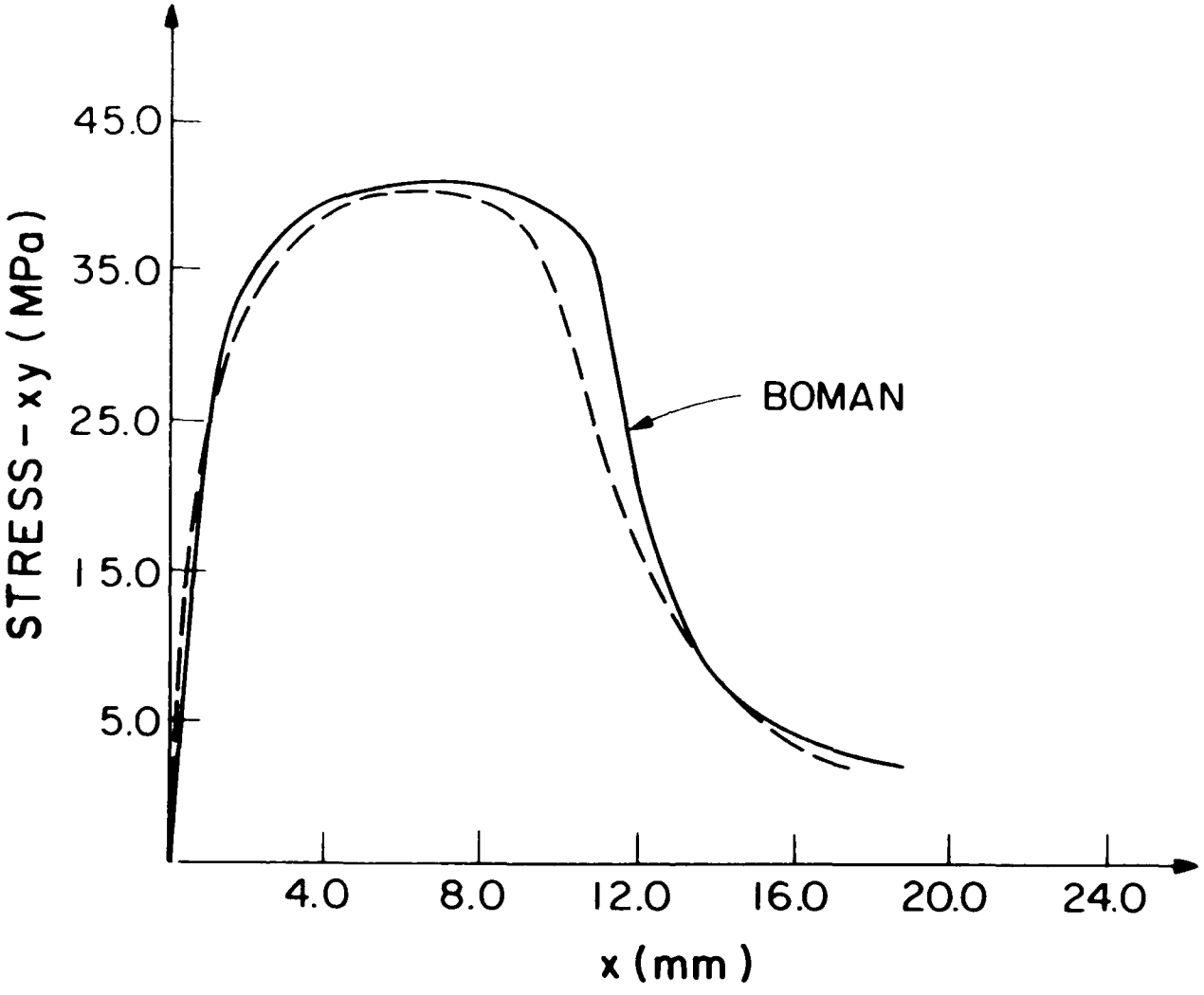

Figure 14 Stresses just below contact surfaces in analysis of wiring around cylinder

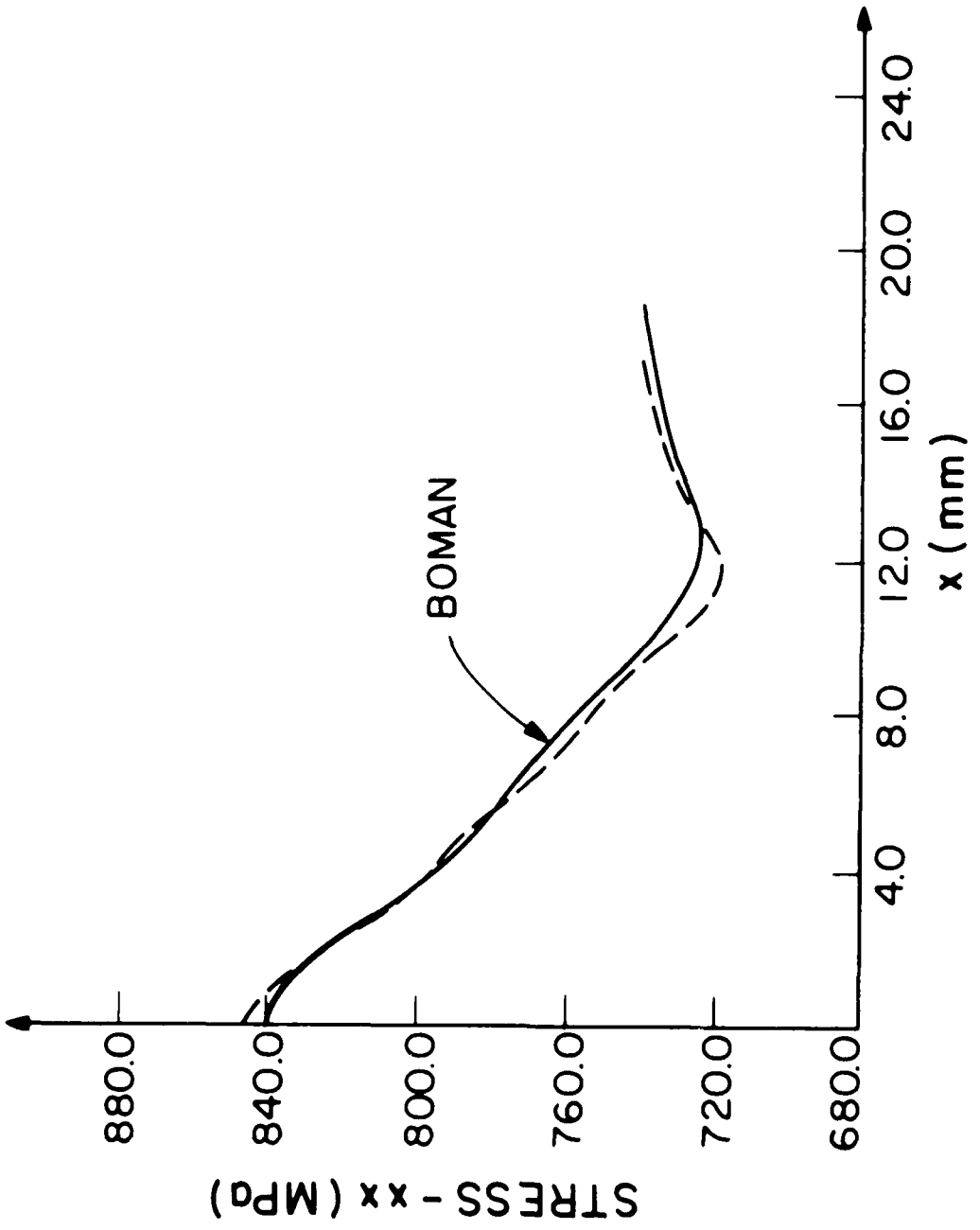

Figure 14, continued

algorithm was obtained using one load step to apply the initial stress σ_{yy} and then two load steps with $\Delta t=1.0$ as shown in Fig. 13 (a) to reach the final stress condition.

4.4 Analysis of a Buried Pipe

Frictional conditions must frequently be modeled in the analysis of soil-structure interactions [15, 23].

Figure 15 shows a pipe buried in soil subjected to the overburden pressure P_0 = 100 kPa. The objective of the analysis was to predict the tractions along the pipe-soil interface. In this analysis, both the pipe and the soil were considered linear elastic media, although in practice the soil may need to be considered nonlinear.

Figure 16 shows the finite element idealization used for the analysis, and Fig. 17 gives the predicted tractions along the contact surface.(+) Also shown in Fig. 17 are the tractions along the interface for the friction coefficients $\mu = 0.0$ and $\mu = \infty$, calculated without the use of the contact algorithm. These results have been obtained by simply using constraint equations so that the pipe and soil nodal displacements are the same perpendicular to the pipe surface, and free tangentially when $\mu = 0.0$ and the same tangentially when $\mu = \infty$.

Figure 17 shows that the results using the contact algorithm are slightly different from those obtained without the contact algorithm. These differences arise mainly because of the traction recovery used in the contact algorithm, and because the contact algorithm always uses the updated nodal point positions (including the displacements) for the contact force calculations, whereas these deformations were neglected when using the constraint equations.

5. CONCLUDING REMARKS

An algorithm for the solution of two-dimensional contact problems, including large deformation and frictional conditions, has been presented. The solution procedure uses a Lagrange multiplier technique to incrementally impose the deformation constraints along the contact surfaces. The contact forces are evaluated from distributed tractions that act on the contactors. The tractions are calculated from the nodal point forces (which correspond to the internal element

(+) As seen in the figure, the figure $\mu = \infty$ can be modeled with the contact algorithm using any large value of μ.

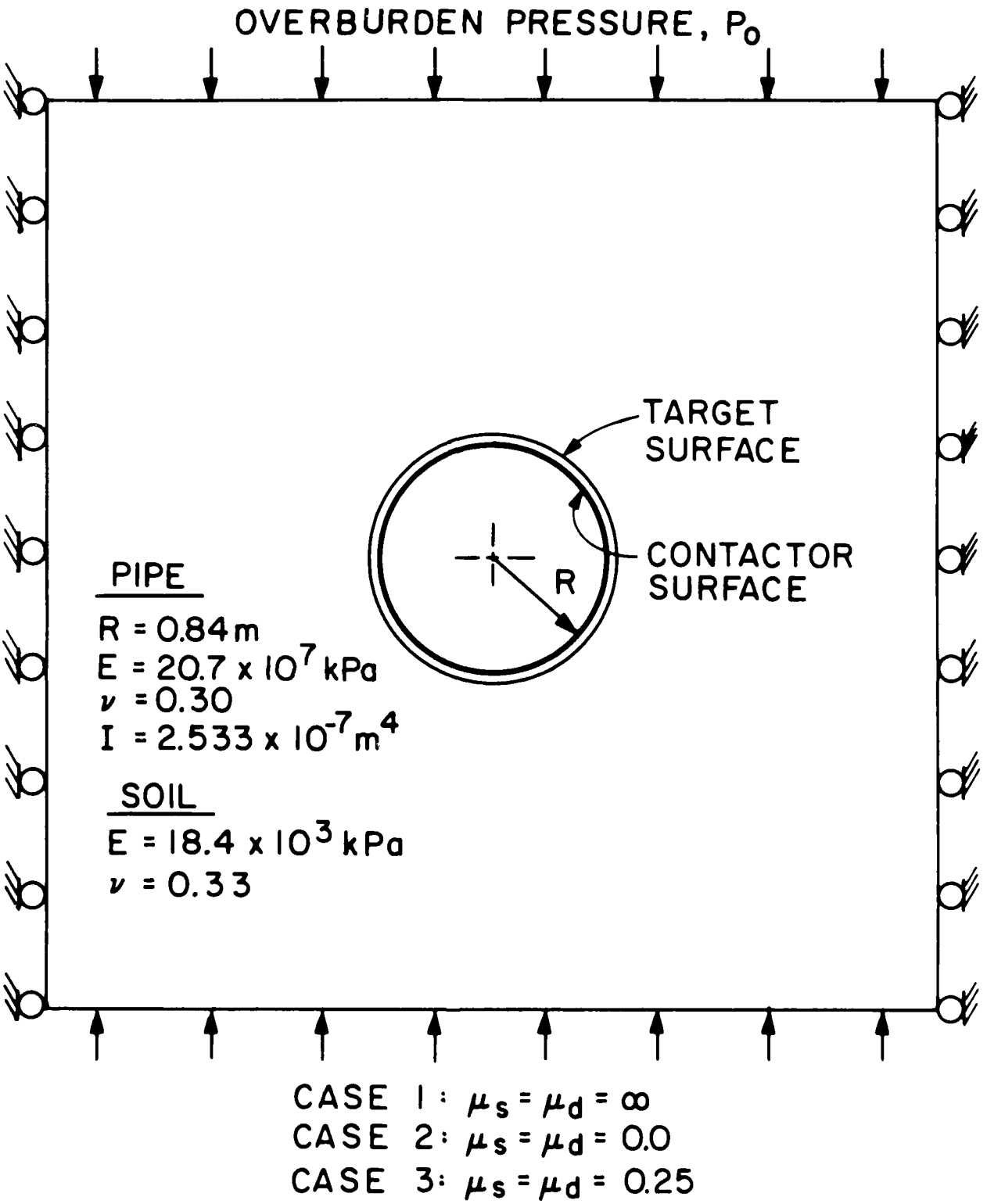

Figure 15 Pipe buried in soil subjected to overburden pressure P_0 = 100 kPa, $\mu = \mu_s = \mu_d$.

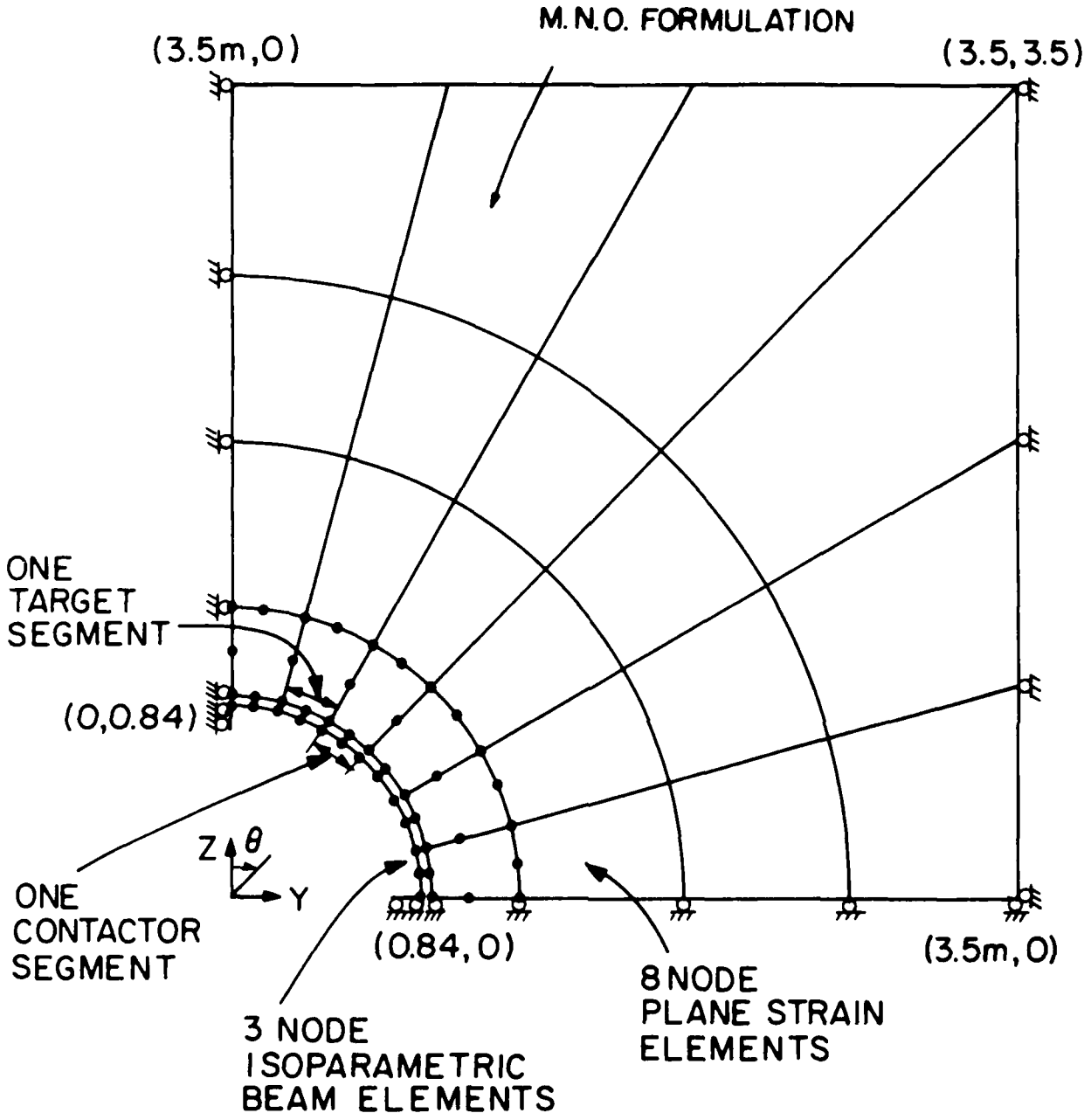

Figure 16 Finite element idealization used for analysis of buried pipe

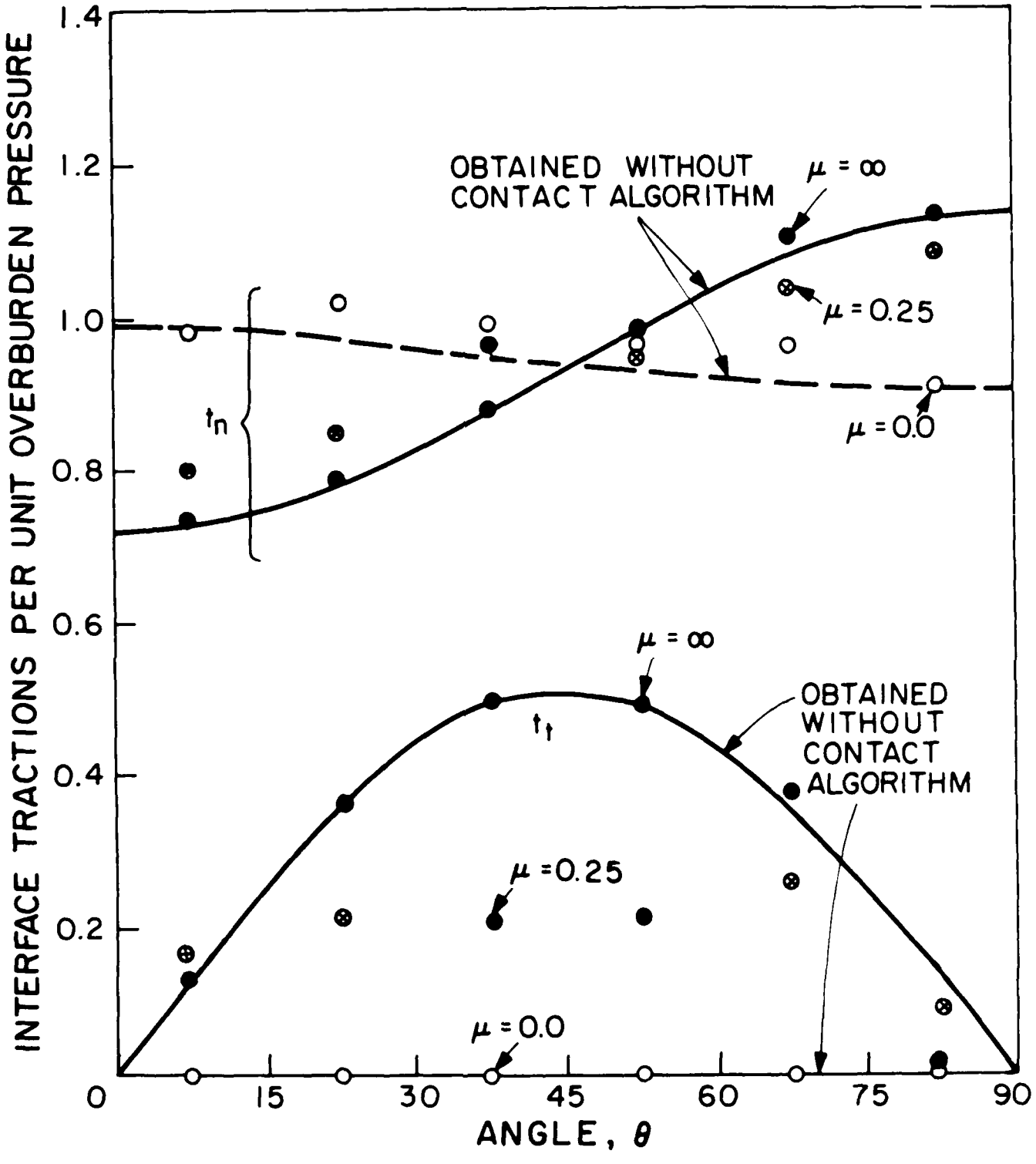

Figure 17 Predicted tractions on pipe/soil interface; solution obtained using four load increments of equal size

stresses and the externally applied loading) and the frictional conditions based on Coulomb's law. The solution results obtained using the algorithm in some contact problems have been presented to demonstrate some of the features of the solution procedure.

Considering the way frictional conditions are accounted for in the algorithm some important assumptions are used. First, the frictional forces in sliding are assumed to act in the same directions as the contact tangential forces prior to sliding. This assumption may require relatively small load increments in the solution. Second, the frictional calculations make only use of the total tangential and normal forces acting on the segments, and do not account for the variation of the tractions over the segments. And third, the relatively simple friction law of Coulomb is employed. A more refined friction law would include rate and state-dependent factors. Using Coulomb's friction law with $\mu_s = \mu_d$ already a large number of contact problems can be modeled using our algorithm, but various questions relating to the physics of motion, and to our numerical solution procedure, must still be addressed when $\mu_s > \mu_d$ [19].

In this first paper, we have concentrated on presenting the theory used and on indicating some applications. Our experiences with the algorithm have been most encouraging, but the field of analysis of contact problems is very large, and many most interesting aspects relating to our algorithm deserve further studies, such as

- the effect of the finite element mesh used for a problem on the performance of the solution procedure;
- effective modeling of the target and contactor bodies, with respect to selection of an appropriate number of contactor and target segments for determination of contact;
- the use of appropriate load incrementation for solution of specific problems, and the effect of different sequences of load application, in particular when $\mu_s > \mu_d$;
- the choice of iteration procedure and convergence criteria (for example, perhaps more effective methods than full Newton iteration can be identified);
- the use of a lumped approach for the traction recovery instead of the consistent approach, and the use of higher-order contact segments;
- rigorous mathematical analyses and convergence studies of the algorithm for frictional conditions.

These studies would be very valuable because they will yield further insight into the solution procedure and provide the basis for improvements of the solution method. We are currently pursuing such studies and plan to report upon them in future communication.

REFERENCES

[1] Chan, C.H., and Tuba, I.S., "A Finite Element Method for Contact Problems of Solid Bodies," Int. J. Mech. Sci., Vol. 13, 1971.

[2] Goodman, R.E., Taylor, R.L., and Brekke, T.L., "A Model for the Mechanics of Jointed Rock," Journal Soil Mechanics and Foundations Division, ASCE, Vol. 94, No. SM3, pp. 637-659, 1968.

[3] Wilson, E.A., and Parsons, B., "Finite Element Analysis of Elastic Contact Problems using Differential Displacements," Int. J. Num. Meth. in Eng., Vol. 2, pp. 387-395, 1970.

[4] Francavilla, A., and Zienkiewicz, O.C., "A Note on Numerical Computation of Elastic Contact Problems," Int. J. Num. Meth. in Eng., Vol. 9, pp. 913-924, 1975.

[5] Cheng, H.S., and Keer, L.M., (eds.), Solid Contact and Lubrication, AMD-Vol. 39, American Society of Mechanical Engineers, 1980.

[6] Hughes, T.J.R., Taylor, R.L., and Kanoknukulchai, W., "A Finite Element Method for Large Displacement Contact and Impact Problems" in Formulations and Computational Algorithms in Finite Element Analysis, (K.J. Bathe et al. eds.), M.I.T. Press, 1977.

[7] Herrmann, L.R., "Finite Element Analysis of Contact Problems," Journal Engineering Mechanics Division, ASCE, Vol. 104, EM5, pp. 1043-1057, 1978.

[8] Okamoto, N., and Nakazawa, M., "Finite Element Incremental Contact Analysis with Various Frictional Conditions," Int. J. Num. Meth. in Eng., Vol. 14, pp. 337-357, 1979.

[9] Urzua, J.L. and Pecknold, O.A., "Analysis of Frictional Contact Problems Using an Interface Element," Proc. Symp. on Appl. of Computer Methods in Eng., Aug. 23-26, Los Angeles, CA, 1977.

[10] Campos, L.T., Oden, J.T. and Kikuchi, N., "A Numerical Analysis of a Class of Contact Problems with Friction in Elastostatics," Comp. Meth. in Appl. Mech. and Eng., Vol. 34, pp. 821-845, 1982.

[11] Oden, J.T. and Pires, E.B., "Nonlocal and Nonlinear Friction Laws and Variational Principles for Contact Problems in Elasticity," ASME, J. Appl. Mech., Vol. 50, pp. 67-76, 1983.

[12] Kalker, J.J., "The Computation of Three-Dimensional Rolling Contact with Dry Friction," Int. J. Num. Meth. Eng., Vol. 14, pp. 1293-1307, 1979.

[13] Kalker, J.J., Allaert, H.J.C. and de Mul, J., "The Numerical Calculation of Contact Problem in the Theory of Elasticity," in Nonlinear Finite Element Analysis in Structural Mechanics, W. Wunderlich et al., eds.) Springer-Verlag, 1981.

[14] Pian, T.H.H. and Kubomura, K., "Formulation of Contact Problems by Assumed Stress Hybrid Elements," in Nonlinear Finite Element Analysis in Structural Mechanics, (W. Wunderlich, et al., eds.) Springer-Verlag, 1981

[15] Desai, C.S., Zaman, M.M., Lightner, J.G., and Siriwardane, H.J., "Thin Element for Interfaces and Joints," Int. J. Anal. and Num. Meth. in Geomechanics, in press.

[16] Bathe, K.J., Finite Element Procedures in Engineering Analysis, Prentice-Hall, 1982.

[17] "ADINA - A Finite Element Program for Automatic Dynamic Incremental Nonlinear Analysis," Report AE 81-1, ADINA Engineering, Watertown, MA 02172, and Vasteras, Sweden.

[18] Dietrich, J.H., "Time-Dependent Friction and the Mechanics of Stick-Slip," Pure and Appl. Geophysics, Vol. 116, pp. 790-806, 1978.

[19] Gu, J.-C., Rice, J.R., Ruina, A.L., and Tse, S.T., "Slip Motion and Stability of a Single Degree of Freedom Elastic System with Rate and State Dependent Friction," Report Mech-41, Division of Applied Sciences, Harvard Univ., March 1983.

[20] Rabinowicz, E., Friction and Wear of Materials, J. Wiley and Sons, 1965.

[21] Timoshenko, S.P. and Goodier, J.N., Theory of Elasticity, McGraw Hill, pp. 409-420, 1970.

[22] Boman, G., Private Communication.

[23] Katona, M., "A Simple Contact-Friction Interface Element with Applications to Buried Culverts," Int. J. Num. and Anal. Meth. in Geomechanics, in press.

DISTRIBUTION LIST

No. of Copies	Organization
12	Administrator Defense Technical Info Center ATTN: DTIC-DDA Cameron Station Alexandria, VA 22314
1	Director of Defense Research & Engineering ATTN: DD/TWP Washington, DC 20301
1	Asst. to the Secretary of Defense (Atomic Energy) ATTN: Document Control Washington, DC 20301
1	Director Defense Advanced Research Projects Agency ATTN: Tech Lib 1400 Wilson Boulevard Arlington, VA 22209
2	Director Federal Emergency Management Agency ATTN: Mr. George Sisson/RF-SR Technical Library Washington, DC 20301
1	Director Defense Intelligence Agency ATTN: DT-2/Wpns & Sys Div Washington, DC 20301
1	Director National Security Agency ATTN: E. F. Butala, R15 Ft. George G. Meade, MD 20755
1	Director Joint Strategic Target Planning Staff JCS Offut AFB Omaha, NB 68113
1	HQDA DAMA-ART-M Washington, DC 20310
1	Director Defense Communications Agency ATTN: 930 Washington, DC 20305
11	Director Defense Nuclear Agency ATTN: DDST/Dr. Conrad SPAS/P. R. Rohr SPSS/K. Goering G. Ullrich SPTD/T. Kennedy SSTL/Tech Lib (2 cys) STSI/Archives STSP/COL Kovel NATD NATA Washington, DC 20305
2	Commander Field Command, DNA ATTN: FCPR FCTMOF Kirtland AFB, NM 87115
1	Commander Field Command, DNA Livermore Branch ATTN: FCPRL P.O. Box 808 Livermore, CA 94550
1	Director Inst for Defense Analyses ATTN: IDA Librarian Ruth S. Smith 400 Army-Navy Drive Arlington, VA 22202
1	Commander US Army Materiel Command ATTN: AMCDRA-ST 5001 Eisenhower Avenue Alexandria, VA 22333
1	Commander US Army Communications Rsch and Development Command ATTN: AMSEL-ATDD Fort Monmouth, NJ 07703

DISTRIBUTION LIST

No. of Copies	Organization
1	Program Manager US Army BMD Program Office ATTN: John Shea 5001 Eisenhower Avenue Alexandria, VA 22333
2	Director US Army BMD Advanced Technology Center ATTN: CRDABH-X CRDABH-S Huntsville, AL 35807
1	Commander US Army BMD Command ATTN: BDMSC-TFN/N.J. Hurst P.O. Box 1500 Huntsville, AL 35807
1	Commander US Army Engineer Division ATTN: HNDED-FD P.O. Box 1600 Huntsville, AL 35807
2	Deputy Chief of Staff for Operations and Plans ATTN: Technical Library Director of Chemical & Nuc Operations Department of the Army Washington, DC 20310
2	Office, Chief of Engineers Department of the Army ATTN: DAEN-MCE-D DAEN-RDM 890 South Pickett Street Alexandria, VA 22304
3	Commander US Army Engineer Waterways Experiment Station ATTN: Technical Library William Flathau Leo Ingram P.O. Box 631 Vicksburg, MS 39180
1	Commander US Army Engineering Center ATTN: ATSEN-SY-L Fort Belvoir, VA 22060
1	US Army MERADCOM ATTN: DRDME-EM, D. Frink Fort Belvoir, VA 22060
1	Commander US Army Armament Research and Development Center ATTN: SMCAR-TDC Dr. Gyorog Dover, NJ 07801
1	Commander US Army Armament Research and Development Center ATTN: SMCAR-TSS Dover, NJ 07801
1	Commanmder US Army Armament Materiel Readiness Command ATTN: AMSMC-LEP-L, Tech Lib Rock Island, IL 61299
1	Director Benet Weapons Laboratory US Army Armament Research and Development Center ATTN: SMCAR-LCB-TL Watervliet, NY 12189
1	Commander US Army Aviation Research and Development Command ATTN: AMSAV-E 4300 Goodfellow Boulevard St. Louis, MO 63120
1	Director US Army Air Mobility Research and Development Laboratory Ames Research Center Moffett Field, CA 94035

DISTRIBUTION LIST

No. of Copies	Organization
1	Commander US Army Communications Rsch and Development Command ATTN: AMSEL-PPA-SA Fort Monmouth, NJ 07703
3	Commander US Army Electronics Research and Development Command Technical Support Activity ATTN: AMDSD-L AMDEW-E, W. S. McAfee AMDSD-EI, J. Roma Fort Monmouth, NJ 07703
8	Commander US Army Harry Diamond Labs ATTN: Mr. James Gaul Mr. L. Belliveau Mr. J. Meszaros Mr. J. Gwaltney Mr. F. W. Balicki Mr. Bill Vault Mr. R. J. Bostak Mr. R. K. Warner 2800 Powder Mill Road Adelphi, MD 20783
4	Commander US Army Harry Diamond Labs ATTN: DELHD-TA-L DRXDO-TI/002 DRXDO-NP DELHD-RBA/J. Rosado 2800 Powder Mill Road Adelphi, MD 20783
1	Commander US Army Infantry School ATTN: ATSH-CD-CSO-OR Fort Benning, GA 31905
1	Commander US Army Missile Command ATTN: AMSMI-R Redstone Arsenal, AL 35898
1	Commander US Army Missile Command ATTN: AMSMI-YDL Redstone Arsenal, AL 35898
1	Commander US Army Missile Command ATTN: Technical Library Redstone Arsenal, AL 35898
4	Commander US Army Natick Research and Development Command ATTN: DRDNA-DT Dr. D. Sieling DRXNE-UE/A. Johnson A. Murphy W. Crenshaw Natick, MA 01760
1	Commander US Army Tank Automotive Command ATTN: AMSTA-TSL Warren, MI 48090
1	Comander US Army Foreign Science and Technology Center ATTN: Rsch & Concepts Br 220 7th Street, NE Charlottesville, VA 22901
1	Commander US Army Logistical Center ATTN: ATCL-SCA Mr. Robert Cameron Fort Lee, VA 23801
3	Commander US Army Materials and Mechanics Research Center ATTN: Technical Library DRXMR-ER, Joe Prifti Eugene de Luca Watertown, MA 02172

DISTRIBUTION LIST

No. of Copies	Organization
1	Commander US Army Research Office P.O. Box 12211 Research Triangle Park NC 27709
4	Commander US Army Nuclear Agency ATTN: ACTA-NAW MONA-WE Technical Library MAJ Uecke 7500 Backlick Rd, Bldg. 2073 Springfield, VA 22150
1	Commander US Army TRADOC ATTN: ATCD-SA, Mr. O. Wells Fort Monroe, VA 23651
2	Director US Army TRADOC Systems Analysis Activity ATTN: LTC John Hesse ATAA-SL, Tech Lib White Sands Missile Range NM 88002
1	Commander US Combined Arms Combat Developments Activity ATTN: ATCA-CO, Mr. L. C. Pleger Fort Leavenworth, KS 66027
1	Commandant Interservice Nuclear Weapons School ATTN: Technical Library Kirtland AFB, NM 87117
1	Chief of Naval Material ATTN: MAT 0323 Department of the Navy Arlington, VA 22217
2	Chief of Naval Operations ATTN: OP-03EG OP-985F Department of the Navy Washington, DC 20350
1	Chief of Naval Research ATTN: N. Perrone Department of the Navy Washington, DC 20360
1	Director Navy Strategic Systems Projects Ofc ATTN: NSP-43, Tech Library Department of the Navy Washington, DC 20360
1	Commander Naval Electronic Systems Com ATTN: PME 117-21A Washington, DC 20360
1	Commander Naval Facilities Engineering Command Washington, DC 20360
1	Commander Naval Sea Systems Command Department of the Navy Washington, DC 20360
3	Officer-in-Charge (Code L31) Civil Engineering Laboratory Naval Constr Btn Center ATTN: Stan Takahashi R. J. Odello Technical Library Port Hueneme, CA 93041
1	Commander David W. Taylor Naval Ship Research & Development Ctr ATTN: Lib Div, Code 522 Bethesda, MD 20084

DISTRIBUTION LIST

No. of Copies	Organization
1	Commander Naval Surface Weapons Center ATTN: DX-21, Library Br. Dahlgren, VA 22448
2	Commander Naval Surface Weapons Center ATTN: Code WA501/Navy Nuclear Programs Office Code WX21/Tech Library Silver Spring, MD 20910
1	Commander Naval Weapons Center ATTN: Code 3433, Tech Lib China Lake, CA 93555
1	Commander Naval Weapons Evaluation Fac ATTN: Document Control Kirtland AFB, NM 87117
1	Commander Naval Research Laboratory ATTN: Code 2027, Tech Lib Washington, DC 20375
1	Superintendent Naval Postgraduate School ATTN: Code 2124, Technical Reports Library Monterey, CA 93940
1	AFSC (Tech Lib)/SDOA Andrews Air Force Base Washington DC 20334
1	ADTC (Tech Lib) Eglin AFB, FL 32542
1	AFATL (DLYV) Eglin AFB FL 32542
1	RADC (EMTLD/Docu Libray) Griffiss AFB, NY 13441
1	AFWL/NTES (R. Henny) Kirtland AFB, NM 87117
1	AFWL/NTE, CPT J. Clifford Kirtland AFB, NM 87117
1	AFWL/SUL Kirtland AFB, NM 87117
1	Commander-in-Chief Strategic Air Command ATTN: NRI-STINFO Lib Offutt AFB, NB 68113
1	AFIT (Lib Bldg. 640, Area B) Wright-Patterson AFB Ohio 45433
1	FTD (TD/BTA/Lib) Wright-Patterson AFB Ohio 45433
1	Director Lawrence Livermore Lab. ATTN: Tech Info Dept L-3 P.O. Box 808 Livermore, CA 94550
2	Director Los Alamos Scientific Lab ATTN: Doc Control for Rpts Lib R. A. Gentry P.O. Box 1663 Los Alamos, NM 87544
2	Director Sandia National Laboratory ATTN: Doc Control for 3141 Sandia Rpt Collection L. J. Vortman Albuquerque, NM 87115
1	Commander US Army Development & Employment Agency ATTN: MODE-TED-SAB Fort Lewis, WA 98433

DISTRIBUTION LIST

No. of Copies	Organization
1	Director Sandia National Laboratory Livermore Laboratory ATTN: Doc Control for Tech Lib P.O. Box 969 Livermore, CA 94550
1	Director National Aeronautics and Space Administration Scientific & Tech Info Fac P.O. Box 8757 Baltimore/Washington International Airport MD 21240
1	Aerospace Corporation ATTN: Tech Info Services P.O. Box 92957 Los Angeles, CA 90009
1	Agbabian Associates ATTN: M. Agbabian 250 North Nash Street El Segundo, CA 90245
1	The BDM Corporation ATTN: Richard Hensley P.O. Box 9274 Albuquerque International Albuquerque, NM 87119
1	The Boeing Company ATTN: Aerospace Library P.O. Box 3707 Seattle, WA 98124
2	California Research and Technology ATTN: M. Rosenblatt F. Sauer 20943 Devonshire Street Chatsworth, CA 91311
1	Carpenter Research Corporation ATTN: H. Jerry Carpenter 6230 Scotmist Drive Rancho Palos Verdes, CA 90274
1	Goodyear Aerospace Corp ATTN: R. M. Brown, Bldg 1 Shelter Engineering Litchfield Park, AZ 85340
2	Kaman AviDyne ATTN: Dr. N.P. Hobbs Mr. S. Criscione 83 Second Avenue Northwest Industrial Park Burlington, MA 01803
3	Kaman Sciences Corporation ATTN: Library P. A. Ellis, F.S. Shelton P.O. Box 7463 1500 Garden of the Gods Road Colorado Springs, CO 80907
1	Kaman Sciences Corporation ATTN: Don Sachs Suite 703 2001 Jefferson Davis Highway Arlington, VA 22202
1	Kaman-TEMPO ATTN: DASIAC P.O. Drawer QQ Santa Barbara, CA 93102
1	Kaman-TEMPO ATTN: E. Bryant, Suite UL-1 715 Shamrock Road Bel Air, MD 21014
1	Lockheed Missiles & Space Co. ATTN: J. J. Murphy, Dept. 81-11, Bldg. 154 P.O. Box 504 Sunnyvale, CA 94086

DISTRIBUTION LIST

No. of Copies	Organization
1	Martin Marietta Corporation Aerospace Division ATTN: G. Fotieo P.O. Box 5837 Orlando, FL 32805
2	McDonnell Douglas Astronautics Corporation ATTN: Robert W. Halprin Dr. P. Lewis 5301 Bolsa Avenue Huntington Beach, CA 92647
2	The Mitre Corporation ATTN: Library J. Calligeros, Mail Stop B-150 P.O. Box 208 Bedford, MA 01730
1	New Mexico Engineering Research Institute (CERF) ATTN: J. Leigh P.O. Box 25 UNM Albuquerque, NM 87131
1	Radkowski Associates ATTN: Peter R. Radkowski P.O. Box 5474 Riverside, CA 92517
2	Physics International ATTN: Technical Library Mr. Fred Sauer 2700 Merced Street San Leandro, CA 94577
2	Union Carbide Corporation Holifield National Laboratory ATTN: Doc Control for Tech Lib Civil Defense Research Project P.O. Box X Oak Ridge, TN 37830
3	R&D Associates ATTN: Jerry Carpenter Technical Library Allan Kuhl P.O. Box 9695 Marina del Rey, CA 90291
1	RCA Government Communications Systems 13-5-2 Front & Cooper Streets Camden, NJ 08102
2	Science Applications, Inc. ATTN: Burton S. Chambers John Cockayne PO BOX 1303 1710 Goodridge Drive McLean, VA 22102
1	Science Applications, Inc. ATTN: Technical Library PO Box 2351 La Jolla, CA 92038
1	Systems, Science and Software ATTN: C. E. Needham PO Box 8243 Albuquerque, NM 87108
3	Systems, Science and Software ATTN: Technical Library R. Duff K. Pyatt PO Box 1620 La Jolla, CA 92037
1	TRW Electronics and Defense ATTN: Benjamin Sussholtz One Space Park Redondo Beach, CA 92078

DISTRIBUTION LIST

No. of Copies	Organization
1	Washington State University Physics Department ATTN: G. R. Fowles Pullman, WA 99163
1	Battelle Memorial Institute ATTN: Technical Library 505 King Avenue Columbus, OH 43201
1	California Inst of Tech ATTN: T. J. Ahrens 1201 E. California Blvd. Pasadena, CA 91109
2	Denver Research Institute University of Denver ATTN: Mr. J. Wisotski Technical Library PO Box 10127 Denver, CO 80210
1	IIT Research Institute ATTN: Milton R. Johnson 10 West 35th Street Chicago, IL 60616
1	TRW Systems Group Ballistic Missile Division ATTN: H. Korman, Mail Station 526/614 P.O. Box 1310 San Bernardino, CA 92402
1	J. D. Haltiwanger Consulting Services B106a Civil Engineering Bldg. 208 N. Romine Street Urbana, IL 61801
1	Massachusetts Institute of Technology Aeroelastic and Structures Research Laboratory ATTN: Dr. E. A. Witmer Cambridge, MA 02139
2	Massachusetts Institute of Technology Mechanical Engineering Dept. ATTN: Prof. K. J. Bathe Dr. Anil Chaudhary Cambridge, MA 02139
2	Southwest Research Institute ATTN: Dr. W. E. Baker A. B. Wenzel 8500 Culebra Road San Antonio, TX 78228
1	SRI International ATTN: Dr. G. R. Abrahamson 333 Ravenswood Avenue Menlo Park, CA 94025
1	Stanford University ATTN: Dr. D. Bershader Durand Laboratory Stanford, CA 94305

Aberdeen Proving Ground

Dir, USAMSAA
ATTN: AMXSY-D
AMXSY-MP, H. Cohen
Cdr/USATCOM
ATTN: AMSTE-TO-F
Cdr/CRDC, AMCCOM,
ATTN: SMCCR-RSP-A
SMCCR-MU
SMCCR-SPS-IL

USER EVALUATION SHEET/CHANGE OF ADDRESS

This Laboratory undertakes a continuing effort to improve the quality of the reports it publishes. Your comments/answers to the items/questions below will aid us in our efforts.

1. BRL Report Number _____ Date of Report _____

2. Date Report Received _____

3. Does this report satisfy a need? (Comment on purpose, related project, or other area of interest for which the report will be used.) _____

_____

_____

4. How specifically, is the report being used? (Information source, design data, procedure, source of ideas, etc.) _____

_____

_____

5. Has the information in this report led to any quantitative savings as far as man-hours or dollars saved, operating costs avoided or efficiencies achieved, etc? If so, please elaborate. _____

_____

_____

6. General Comments. What do you think should be changed to improve future reports? (Indicate changes to organization, technical content, format, etc.)

_____

_____

_____

CURRENT ADDRESS

_____
Name

_____
Organization

_____
Address

_____
City, State, Zip

7. If indicating a Change of Address or Address Correction, please provide the New or Correct Address in Block 6 above and the Old or Incorrect address below.

OLD ADDRESS

_____
Name

_____
Organization

_____
Address

_____
City, State, Zip

(Remove this sheet along the perforation, fold as indicated, staple or tape closed, and mail.)

FOLD HERE

Director
US Army Ballistic Research Laboratory
ATTN: AMXBR-OD-ST
Aberdeen Proving Ground, MD 21005-5066

NO POSTAGE
NECESSARY
IF MAILED
IN THE
UNITED STATES

OFFICIAL BUSINESS
PENALTY FOR PRIVATE USE. $300

BUSINESS REPLY MAIL
FIRST CLASS PERMIT NO 12062 WASHINGTON, DC
POSTAGE WILL BE PAID BY DEPARTMENT OF THE ARMY

Director
US Army Ballistic Research Laboratory
ATTN: AMXBR-OD-ST
Aberdeen Proving Ground, MD 21005-9989

FOLD HERE

END

FILMED

2-85

DTIC